Fall 2016

Reduction of EMI due to common mode current using common mode filter or lossy material

Qian Liu

Department:

REDUCTION OF EMI DUE TO COMMON MODE CURRENT USING COMMON MODE FILTER OR LOSSY MATERIAL

by

QIAN LIU

A THESIS

Presented to the Faculty of the Graduate School of the

MISSOURI UNIVERSITY OF SCIENCE AND TECHNOLOGY

In Partial Fulfillment of the Requirements for the Degree

MASTER OF SCIENCE IN ELECTRICAL ENGINEERING

2016

Approved by

Victor Khilkevich, Advisor
David J. Pommerenke
Jun Fan

PUBLICATION THESIS OPTION

This thesis consists of the following four papers, formatted in the style used by the Missouri University of Science and Technology, listed as follows:

Page 2-25 are intended for submission to the IEEE TRANSATIONS ON ELECTROMAGNETIC COMPATIBILITY.

Page 26-42 are intended for submission to the IEEE LETTER ON ELECTROMAGNETIC COMPATIBILITY.

Page 43-60 are intended for submission to the IEEE INTERNATIONAL CONFERENCE ON ELECTROMAGNETIC COMPATIBILITY.

Page 61-75 are intended for submission to the IEEE INTERNATIONAL CONFERENCE ON ELECTROMAGNETIC COMPATIBILITY.

ABSTRACT

This thesis consists of four papers. In the first paper, two new common mode filter structures were designed, fabricated, and measured. A "sandwich-type" EBG structure that resonates at the desired filter frequency is designed to suppress common mode filter on differential signals. The new filters are placed on top of the PCB as a surface-mount component, instead of being implemented within the PCB stackup. The total radiated power (TRP) of the implemented filter is investigated and discussed. RF absorbing material and traditional shielding are considered to reduce the TRP.

In the second paper and third paper, new PCB-embedded common mode filters are designed and investigated. Based on a quarter-wavelength resonator, an inter-digital structure is designed having an electrical size of only $0.15\ \lambda \times 0.065\ \lambda$, where λ is the effective wavelength in the CM filter. Its interdigital structure is also capable of suppressing higher order harmonics of the CM signal and can be used for USB 3.0 to mitigate electromagnetic interference. Further, a novel broadband suppression structure is described that uses magnetically lossy material to suppress the CM signal from 4.6 to 20 GHz without strongly affecting the intended differential signal.

In the fourth paper, a methodology for validating the parameters of magnetic absorbing materials was developed. The microstrip line test can be recommended as an easy-to-implement validation method for the measured material parameters. The heat sink model and simulation comparison has also been investigated to determine the radiation mitigation with lossy materials.

ACKNOWLEDGMENTS

I would like to express my sincere gratitude to Dr. Victor Khilkevich, my advisor, for his guidance and instruction on my research work, financial support to my study and direction for this thesis during my pursuit of the Master's degree. I learned not only academic knowledge from Dr. Khilkevich, but also the rigorous attitude, good manners, and courage to face difficulties.

I would like to thank Dr. Jun Fan, Dr. David Pommerenke and Dr. James Drewniak for their teaching in my courses, discussions related to my research and helpful suggestions on my thesis.

I would also like to express my thanks to all the other faculty members and students in and out of the EMC lab for their team work and help in my coursework and research.

Finally, my heartfelt gratitude goes to my parents and my husband, Sen Yang, for their support and encouragement towards achieving this goal.

TABLE OF CONTENTS

LIST OF ILLUSTRATIONS

Page

PAPER I

PAPER II

LIST OF TABLES

Page

1. INTRODUCTION

In the real world, small asymmetries in the differential pair can have a large impact on electromagnetic compatibility (EMC) and signal integrity (SI) if not handled properly. The discontinues will dramatically increase the amount of common mode (CM) noise seen at the receiver, increases the emissions from the CM current and thus interference and crosstalk problems. Paper I, Paper II and Paper III will discuss different kind of common mode filter. The filter can be used in the printed circuit board and suppress the common at the desireable frequency, which can decrease EMI.

Absorbing materials for reduction of electromagnetic interference (EMI) are typically used at later stages of electronic product development as a practical countermeasure to possible regulatory issues. Design consideration for absorbing materials at earlier stages could be beneficial to provide cost-effective solutions. Paper IV gives a method to get the material parameters and vidation. Knowing the permeability (μ) and permittivity (ε) of the lossy material to be able to choose the appropriate material from a number of available candidates and predict the performance of the EMI mitigation solution. Finally, measurement and simulation are done to investigate the sheilding effectiness of the lossy material.

PAPER

I. REDUCTION OF EMI DUE TO COMMON MODE CURRENTS USING A SURFACE-MOUBT, EBG-BASED FILTER

Qian Liu, *Student Member, IEEE*, Sam Connor, *Senior Member, IEEE*, Carlo Olivieri, *Member, IEEE*, Francesco de Paulis, *Member, IEEE*, Antonio Orlandi, *Fellow, IEEE*, Michael Cracraft, *Member, IEEE*, Bruce Archambeault, *Fellow, IEEE*, Victor Khilkevich, *Member, IEEE*

ABSTRACT

Common mode (CM) noise on differential signals can be suppressed by planar Electromagnetic Band-gap (EBG) technologies. In this work, two new common mode filter structures were designed, fabricated, and measured. The filters are based on a previously proposed geometry, a "sandwich-type" EBG structure that resonates at the desired filter frequency; however, the new filters are placed on top of the PCB as a surface-mount component, instead of being implemented within the PCB stackup. Stripline and microstrip versions of the removable filter are considered. The filters can be easily removed and substituted with another one that is designed to filter a different frequency but maintains the same footprint and external dimensions. In addition, the surface-mount filter allows us to incorporate DC blocking capacitors into the microstrip version of the filter, thus providing two functions in one package. The total radiated power (TRP) of the implemented filter is investigated and discussed. RF absorbing material and traditional shielding are considered to reduce the TRP.

Index Terms— Electromagnetic band-gap structures (EBG), common mode filter, common mode (CM), differential pair, narrowband filter.

1. INTRODUCTION

Common mode (CM) noise often induces electromagnetic interference (EMI) problems. It is caused by imbalances in the differential signal and/or its path [1]. The increasing bit rate of modern high speed digital electronics leads to increased EMI problems, such as unwanted radiation to the surrounding environment and coupling to nearby active and passive devices [2]. Common mode current is recognized as a major source of radiation and can ultimately deteriorate the signal quality, therefore differential interconnects have to be designed carefully to minimize any source of imbalance (i.e. amplitude mismatch, rise/fall time difference). From an EMI point of view, any CM current flowing on differential interconnects will radiate to some extent. Radiation from differential wiring on printed circuit boards (PCB) can be mitigated by burying the signals on internal layers or by placing the PCB within a shielded enclosure, but when the signals exit the PCB on an I/O cable, the cable may become radiating structure. The cables can be shielded as well, and often are, but the connection between chassis and cable shield presents an opportunity for leakage. The best way to mitigate the emissions from a cable assembly is to attenuate the CM currents significantly before the signals exit the PCB and enter the cable [3].

Common mode filters are widely used to attenuate common mode noise, while ensuring the intentional differential signal is unaffected [4]-[7]. The basic filter principle relies on coupling the common mode energy on the differential traces into resonant cavities while ensuring the unperturbed propagation of the intentional differential signal. These common mode filters can be built on a PCB with typical planar technologies [8]-[12]. Recent studies have focused on the filters that are easy to design and to fabricate. The filter needs to be compact to be attractive to designers of high density PCBs. These practical constraints led us to replace the simple planar patch cavity with an EBG sandwich-type resonant structure [13]-[19].

A further advancement is proposed in this paper: the differential pair transitions up onto a surface-mount component. This minimizes the impact on the PCB design, because the solid reference planes are not being etched into periodic patterns, thereby preventing noise coupling from one cavity into another and also eliminating any concerns

with power distribution due to increased IR drop. The idea is to create a standalone filter that can be easily installed to and removed from the PCB through pads on the PCB's outer layers. Given a certain footprint on the PCB, a different resonant frequency can be obtained by choosing the permittivity of the dielectric and the EBG's geometric parameters appropriately. The main drawback with this approach is the variability in separation distance due to soldering processes, but this drawback is minimized by keeping the signals and EBG patches off of the bottom layer of the removable part. Another novel advancement in this paper is that DC blocking capacitors can be placed on the removable component if the filter is designed with microstrip lines on the top surface. In this embodiment, two functions are performed by one standalone component.

A detailed investigation of the electromagnetic behavior of this filter structure is shown below. This work extends the previous studies in [17]-[20], considering the total radiation issue. Measurement and simulation results are compared to validate the performance of the removable EBG filter and its design process. Total radiated power is measured and compared to determine the effectiveness of the standalone filter. In addition, both RF absorbing material and traditional shielding are explored as methods of mitigating the added radiation from the removable filter.

2. INSPIRATION AND DESIGN CONCEPT

The original proposed EBG structure is shown in Figure 2.1 (a) [17]. The common mode energy will couple into the cavity when the return current reaches the gaps between adjacent EBGs, reducing the amount of common mode that reaches the receiver. However, the currents associated with the differential signal pass over the filter unaffected.

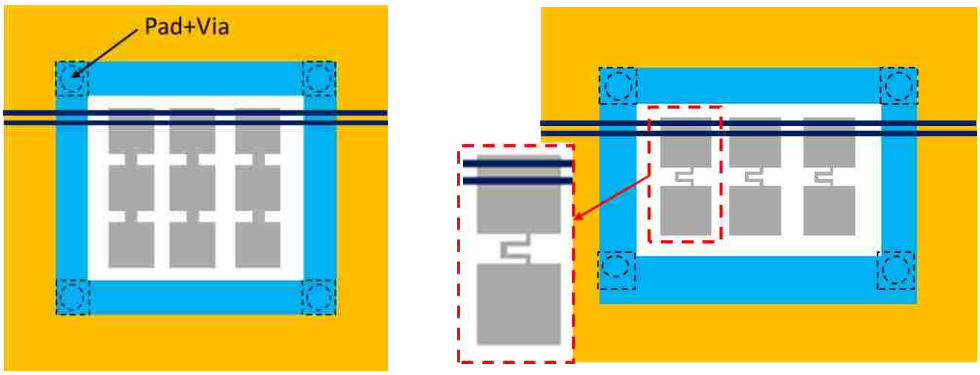

(a) (b)

Figure 2.1. Top view of the EBG configuration: (a) "original" configuration, (b) with meandered bridges between the patches.

The central patch in the three patches of the original configuration was found to be unimportant for the construction of a resonant cavity. In order to reduce the required EBG space, the central patch is replaced by a serpentine trace (called a meandered bridge in previous papers) which links the remaining two patches, as shown in Figure 2.1(b). A further size reduction is achieved by folding this structure into a "sandwich-type" configuration. Figure 2.2 shows the top view and stackup of the EBG "sandwich" geometry. By introducing two more layers, one row of patches stays on the layer directly below the traces, but the other row of patches is placed on another layer with a solid reference layer in between (Figure 2.2 (b)). The patches on different layers are connected with each other by vias, and antipads are used to isolate the vias from the intermediate reference plane.

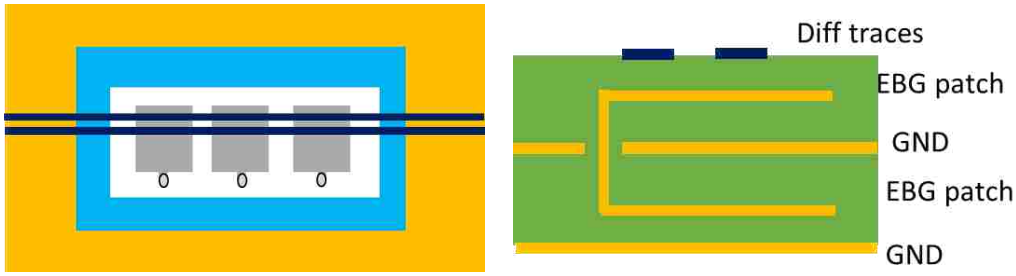

(a) (b)

Figure 2.2. EBG configuration with a "sandwich" structure: (a) top view, (b) related stack-up.

The miniaturized “sandwich-type” EBG described briefly above and more thoroughly in [17] is combined with the idea of a removable, surface-mount filter [20]. This combination provides good design flexibility, limited costs, and a compact component. The sandwich structure proposed in [17] could be considered unattractive since it employs four PCB layers instead of two as in the original planar configuration, but the combination of the sandwich EBG together with the removable part concept makes this filter viable. The cost increase due to the more complex component stack-up and the possible use of expensive laminate material is limited to the small filter footprint instead of to the PCB as a whole. One limitation during the design process is that the EBG design procedure presented in [21]-[22] cannot be directly applied to the sandwich type of layout. The analytical method is only applied to calculate a preliminary patch and via sizing; then a refinement process must be performed to achieve the target frequency. The vias are kept as close as possible to the patch in order to minimize the filter area. Therefore, the tuning involves adjusting the patch size and the position of the vias with respect to the patch edge, which is a different approach than our previous work and which always kept the patch to patch connection in the center of the patch edge. The final layout geometry and the filtering performance are discussed in Section 3.

3. SIMULATION AND MEASUREMENT RESULT ANALYSIS

Based on the concept explored above, corresponding filter and PCB structures were fabricated and simulated using a 6 layer, Megtron 6 laminate ($\varepsilon r \approx 3.58$, $tg\ \delta \approx 0.004$ at 10 GHz) with stackup information described in Figure 3.1. Filters with stripline and microstrip traces are both considered. DC blocking capacitors are added when microstrip lines are used. The filters are attached to the motherboard with a stencil and solderpaste process. The physical dimensions of the fabricated filter are shown in Table 3.1.

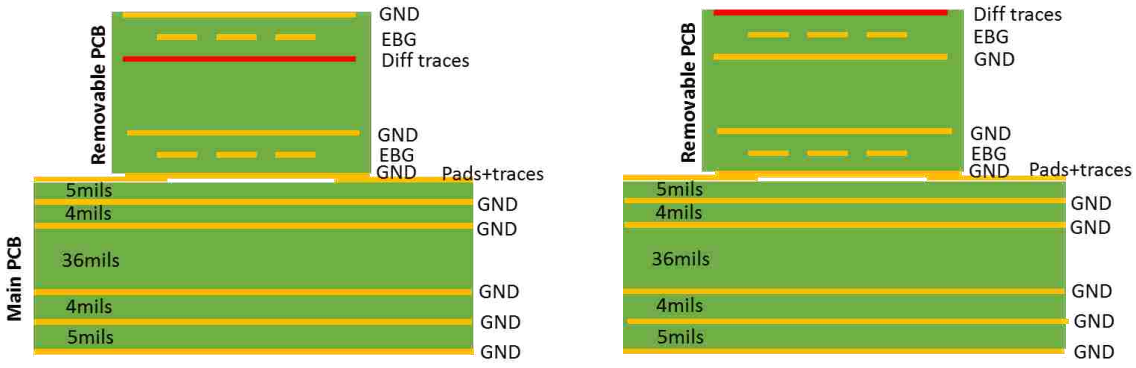

(a) (b)

Figure 3.1. Stackup cross section of removable "sandwich" EBG: (a) stripline, (b) microstrip line.

Table 3.1. A list of the physical dimensions of the fabrications of the EBG filters.

Parameters	Stripline (Figure 3.2)	Microstrip (Figure 3.3)
w	4.57 mm	4.57 mm
g	1.35 mm	1.31 mm
L	9.56 mm	9.56 mm
d	1.35 mm	1.31 mm
L_dieletric	0.7 mm	1.2 mm
gap	0.55 mm	0.45 mm

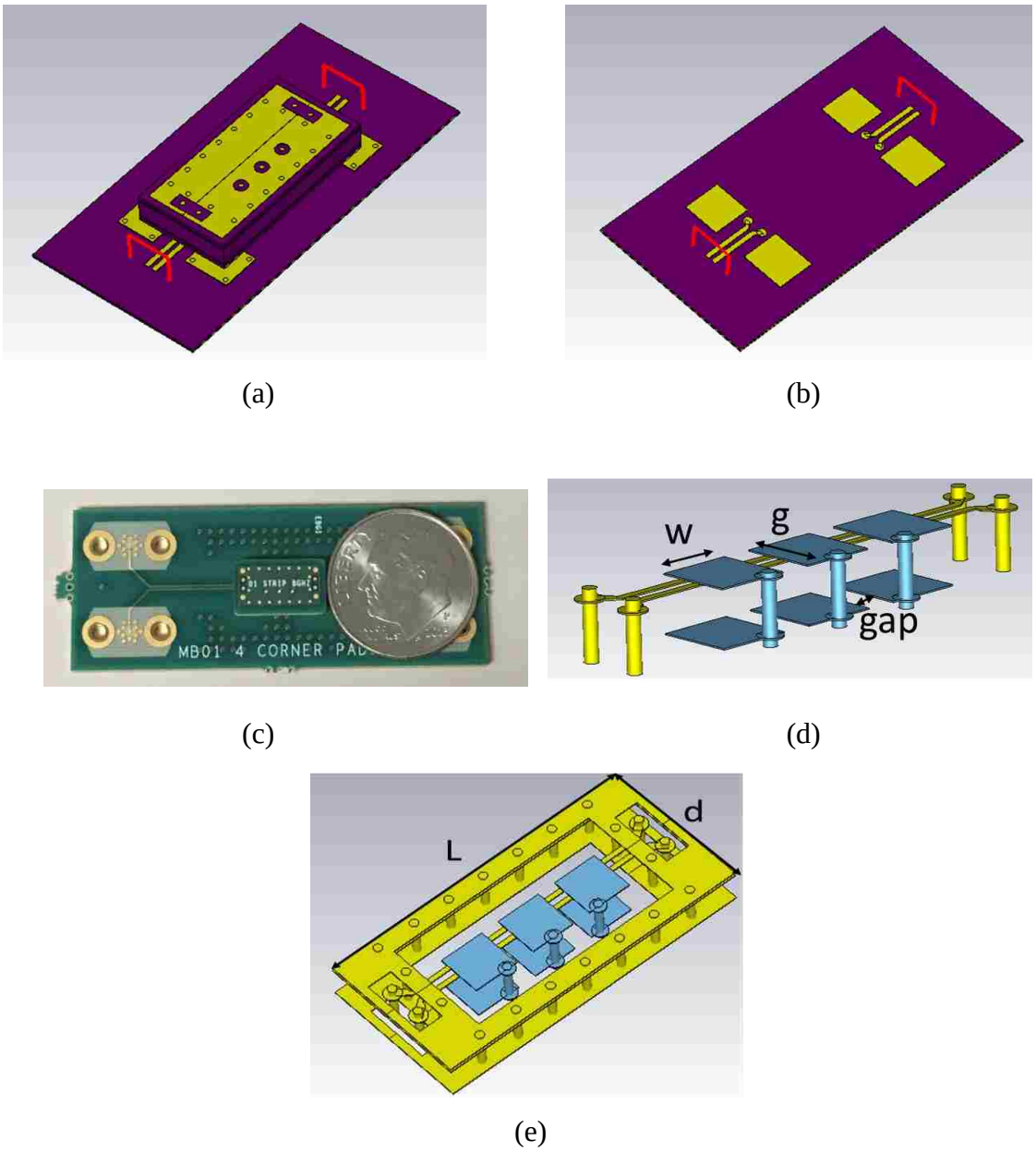

Figure 3.2. Removable "sandwich" EBG configuration (stripline): (a) isometric view, (b) mother board, (c) a photograph of filter and PCB motherboard compared with one U.S. dime (17.9mm diameter), (d) EBG patches and differential trace (e) EBG patches, differential trace and ring.

Three-dimensional, full-wave simulation models were built in CST [23] to study the filter performance, and several views of these models are shown in Figure 3.2- Figure 3.4. The motherboard, shown in Figure 3.2 (b), is exactly the same for all cases. The

motherboard utilizes the top layer for differential traces and pads and the other five layers are solid reference planes, connected by plated through-holes in each corner of the device. Cutaway views of the removable EBG boards are shown in Figure 3.2 (d)-(e) and Figure 3.4 (b)-(c) to provide a better understanding of the "sandwich" geometry. The solid reference planes in the removable part, which are layers one, four and six for stripline and layers three, four and six for microstrip, are shown in Figure 3.3. The vias with circular antipads are used to connect the EBG patches, and the via pairs in the rectangular antipads are used to bring the differential signals from the bottom layer to the top or third layer of the filter board.

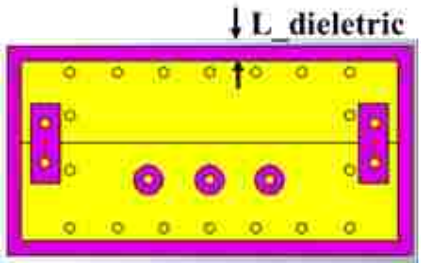

Figure 3.3. Top view of removable part: layer one, four and six for stripline, layer two, four and six for microstrip line.

The manufactured motherboard features launches for a surface-mount 2.9 mm SMK connector. These launches have been designed to minimize return and insertion losses. The microstrip traces have 50 Ohm singled ended characteristic impedance and 85 Ohm differential characteristic impedance. The measurement and simulation results are compared in Figure 3.5 for stripline and in Figure 3.6 for microstrip. The test boards are measured with a calibrated 4-port VNA to observe the $S_{CC}21$ and $S_{DD}21$ of the differential pair. Both measured results were de-embedded using the SFD (smart fixture de-embedding) method [24] to remove the effect of the connector transitions. Both the filters are designed for an 8 GHz resonance, however, due to underestimation of the dielectric permittivity ($\varepsilon r \approx 3.2$ in design but $\varepsilon r \approx 3.6$ for manufacture), the primary resonance shifted from 8 GHz to 7.35 GHz for stripline and to 7.45 GHz for microstrip.

The difference in the loss characteristics of the laminate also accounts for the magnitude difference in $S_{DD}21$ and the attenuation difference in $S_{CC}21$. However, this highlights another benefit of placing the filter in a removable part. Only the removable part needs to be modified to adjust the filter frequency; no change to the motherboard is required. The results indicate that both filters have 900 MHz bandwidth for 5 dB filter notch depth and 700 MHz bandwidth for 10 dB depth. In addition, adding the DC blocking capacitors to the differential pair in the removable part will not affect the performance of differential signaling (Figure 3.6 (b)).

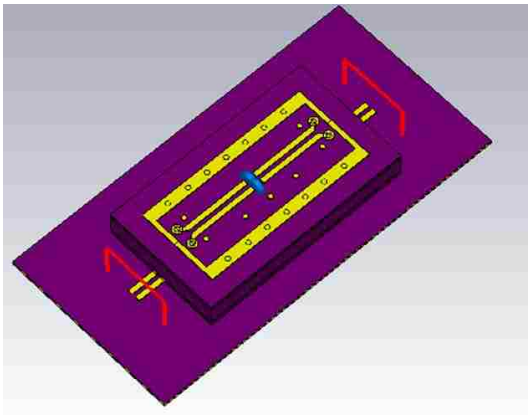

(a)

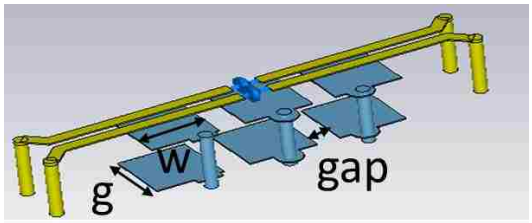

(b)

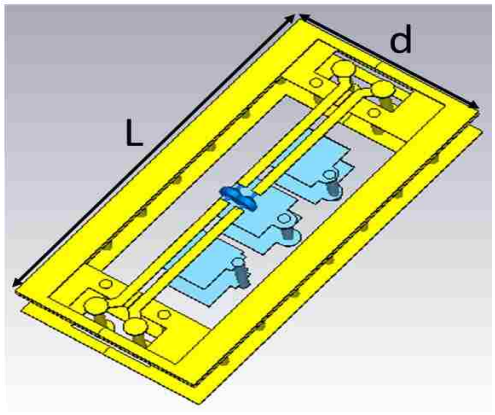

(c)

Figure 3.4. Removable "sandwich" EBG configuration (microstrip line): (a) isometric view, (b) EBG patches and differential trace (c) EBG patches, differential trace and rings.

When the filter parts are cut out of the manufactured PCB panel, some amount of extra dielectric remains around the perimeter of the removable part, illustrated by the pink border region in the CST model shown in Figure 3.3. This dielectric border around the removable part does not affect the primary resonance but does affect the second resonance frequency. As common mode energy couples into the plane cavity, the width of the dielectric border (L_dieletric) will affect the fringing field distribution.

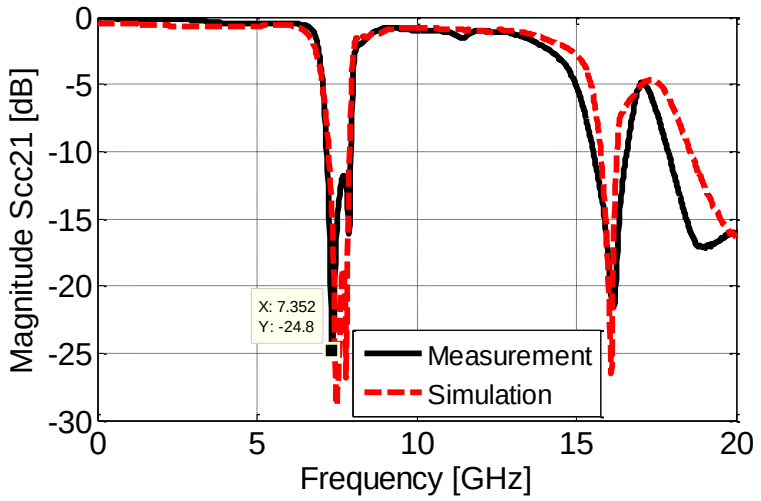

(a)

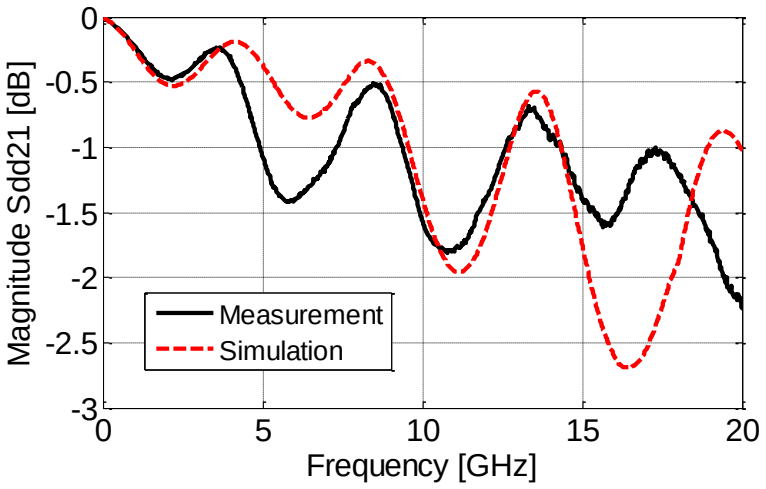

(b)

Figure 3.5. Stripline's simulated and measured S-parameter comparison: (a) $S_{cc}21$, (b) $S_{dd}21$.

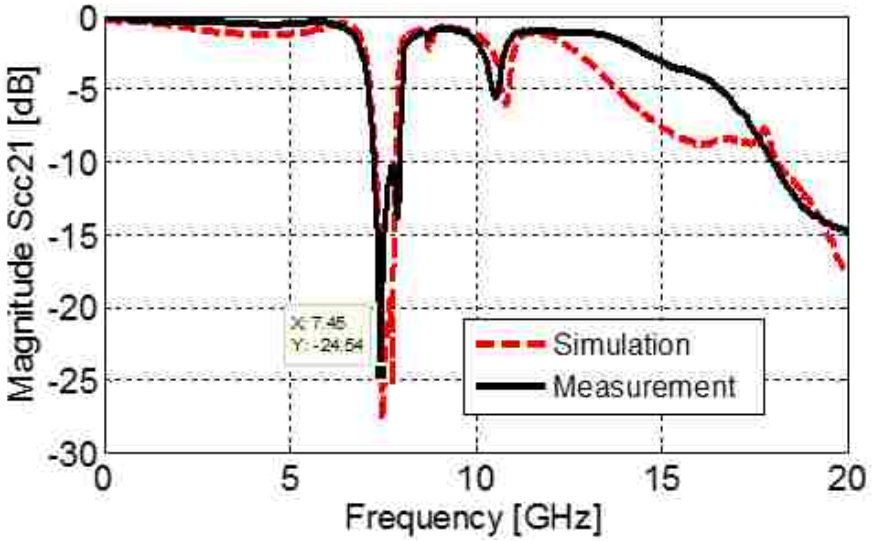

(a)

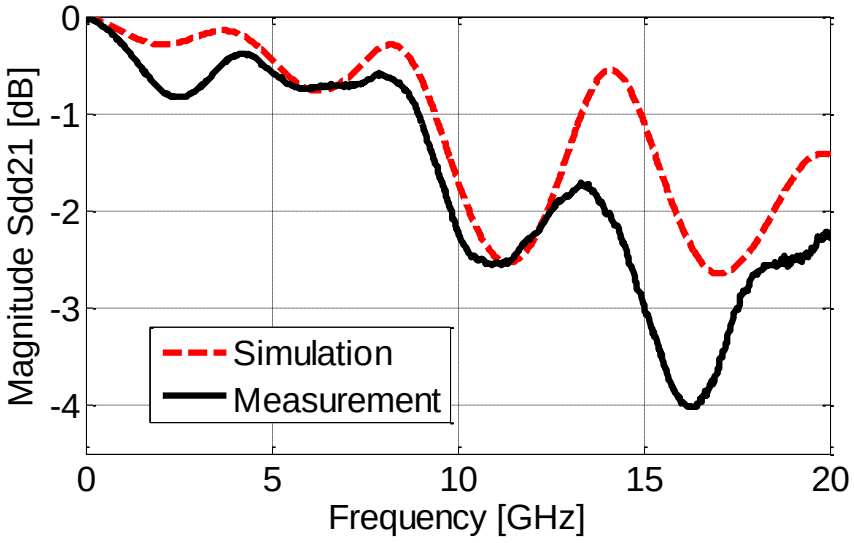

(b)

Figure 3.6. Mcrostrip line's simulated and measured S-parameter comparison: (a) $S_{cc}21$, (b) $S_{dd}21$.

Figure 3.7 provides the physical dimensions of the manufactured EBG patches. Once the dielectric and stackup is determined, the filtering frequency of the removable filter can be modified by adjusting the patch dimensions and the via locations on the patches.

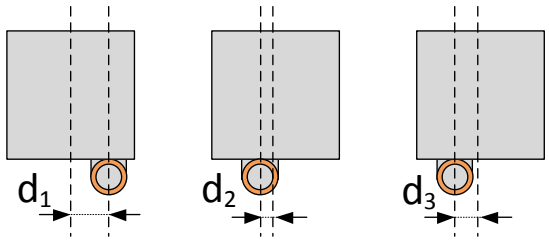

Figure 3.7. Top view of surface-mount EBG patches showing the relative positions of the connection vias for both the models in Fig.3.2 and Fig.3.4.

The models for the microstrip and stripline cases which are based on the originally designed centered vias are modified to study the via location effect on the notch depth and bandwidth. The change in the via location impacts the EBG cavity inductance. Thus, one would expect that by modifying one or two patch vias, separate notches should be achieved. If these notches are close enough, such that the inter-notch profile does not move up exceeding the -10dB limit, the filter bandwidth will be expanded compared to the original centered-vias case.

This via variation is investigated on both the microstrip and stripline cases. As shown in Figure 3.8 (a), the particular the centered-via stripline case (d1=d2=d3=0) has

-14 dB filtering notch; by moving the two lateral patch vias up to 19 mils (480 um) from the inner patch edge, the notch depth reaches -30 dB and has larger 10dB bandwidth. A 7 mils variation (reaching 12 mils from the patch inner edge) provides better response with the two notches being distinguishable which offers 640 MHz bandwidth at -10dB. The final manufacture stripline uses d1=d3=12mils and d2=0 case.

Similar effect is observed on the microstrip case shown in Figure 3.8 (b). The original centered-via case has the single notch reaching only -16 dB. After moving only the via of right patch (d3= 18.5mils distance from the patch inner edge), the notch are drastically improved to -50dB. A similar change from the original case is made by varying the distance between the via and the left patch, d1=13 mils, this leads to the notch separation, with a maximum depth of -37dB. Since reasonable values for common mode reduction are in the range of -10 to -20 dB, and thus -37 dB is even too large, a further modification is applied. By combining the two cases proposed above the microstrip line case is changed to an asymmetrical configuration. The final layout

(d1=13mils, d2=3mils, d3=8mils) offered the good response in terms of notch bandwidth, with 680 MHz bandwidth at -10dB.

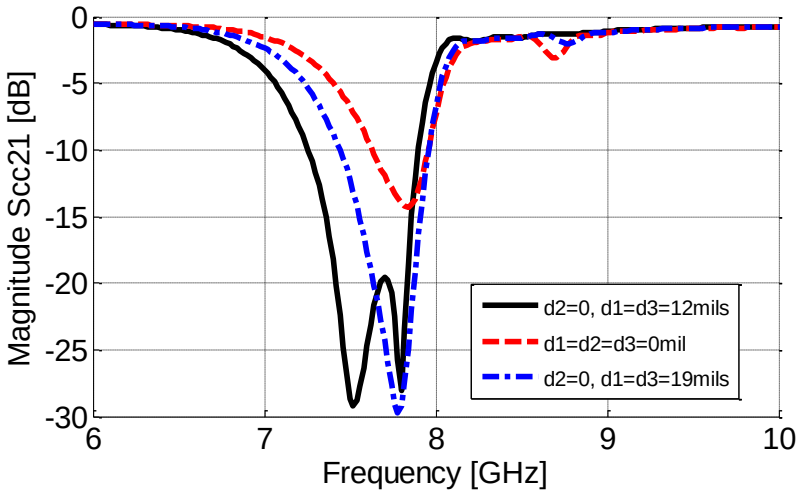

(a)

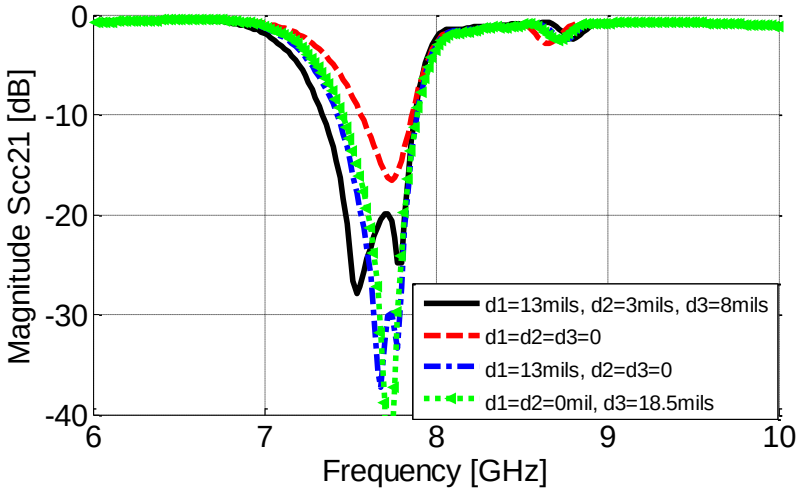

(b)

Figure 3.8. Simulation results coming from the different placements of the connection vias in both the R-EBG structures: (a) stripline (model from Fig.3.2) and (b) microstrip (model from Fig.3.4).

4. ANALYSIS OF TOTAL RADIATED POWER

Total radiated power (TRP) is one of the main concerns in EBG design. Due to the discontinuities introduced by the filter, a part of the signal energy is radiated and could cause coupling or emissions problems. In order to quantify the radiation increase of adding a removable filter, both filters are tested in a reverberation chamber with a common mode excitation. All the TRP measurement results in this section are normalized to 1 Watt excitation for the comparison purposes. The far-end ports are terminated with 50 Ohm loads. Figure 4.3 compares the results of the TRP measurements. The reference board is the differential pair on the first layer of the mother board without the removable part. The results indicate that both stripline and microstrip line filters contribute about 23 dB more TRP at the peak around 11 GHz compared to the reference board.

An investigation of the electric field distribution at resonant frequencies in the S-parameters response is shown in Figure 4.1 for stripline and in Figure 4.2 for microstrip line. Figure 4.1 (a) and Figure 4.2 (a) indicate that the primary resonances are due to the EBG patches. The resonance around 11 GHz is caused by the plane resonance between the removable part and the mother board (Figure 4.2 (b)). For the resonance around 16 GHz, the ring resonances are excited by the vertical current, which has been investigated in previous studies [20].

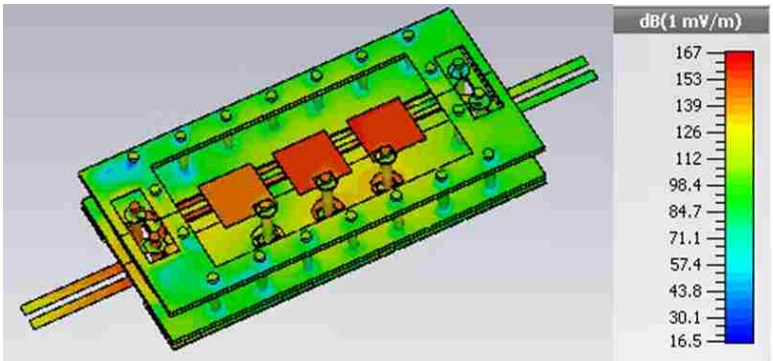

(a)

Figure 4.1. Spatial distribution of the magnitude of E-Field on the removable EBG — stripline: (a) 7.35 GHz and (b) 16.08 GHz.

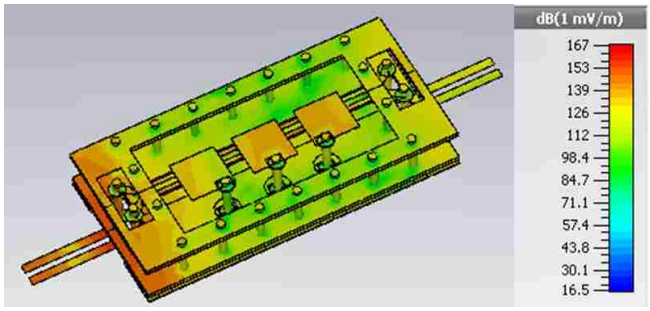

(b)

Figure 4.1. Spatial distribution of the magnitude of E-Field on the removable EBG — stripline: (a) 7.35 GHz and (b) 16.08 GHz. (cont.)

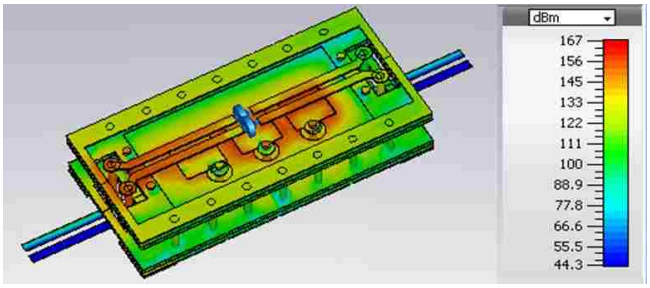

(a)

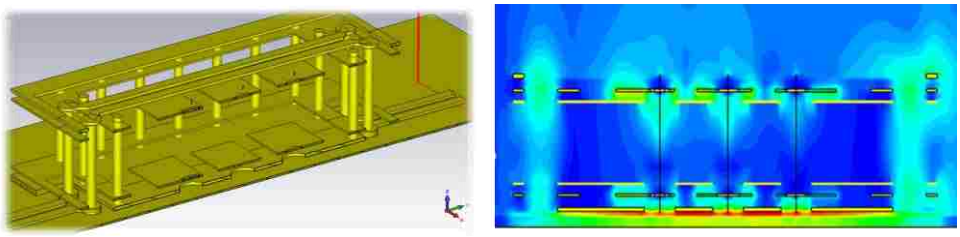

(b)

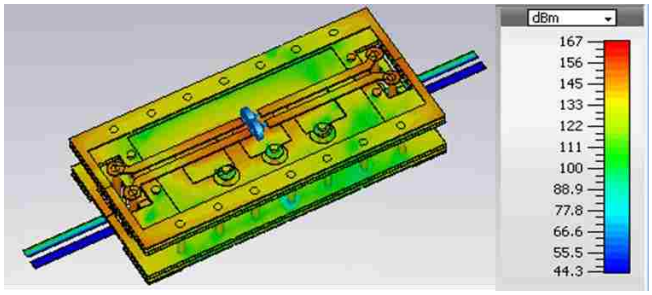

(c)

Figure 4.2. Spatial distribution of the magnitude of E-Field on the removable EBG— microstrip line: (a) 7.45 GHz, (b) 10.08 GHz and (c) 16 GHz.

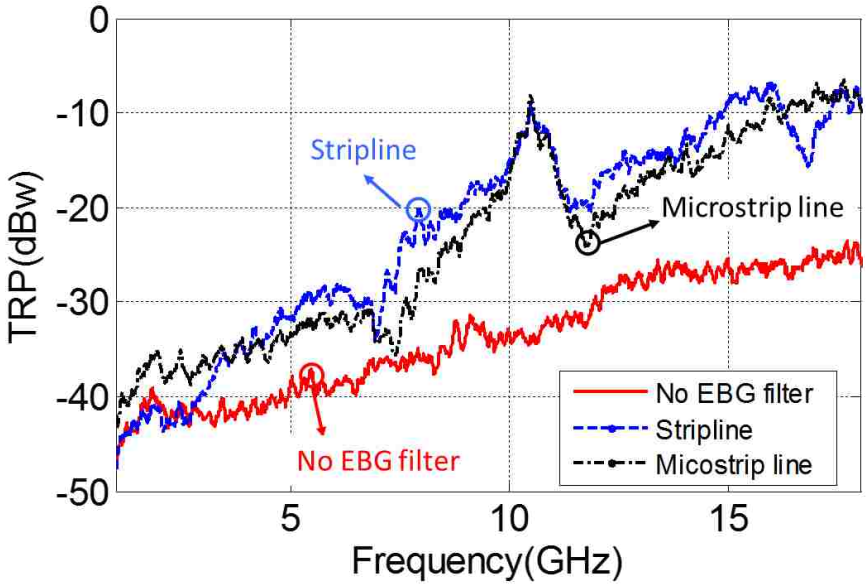

Figure 4.3. Measured TRP results comparison.

In order to reduce the impact of increased radiation, a solution of applying radio frequency absorbing material, hereafter called 'lossy material,' is considered. Because the electric field distribution suggests that the peak radiation around 11 GHz is due to the plane resonance, we applied a picture frame of lossy material configuration around the EBG filter. Figure 4.4 illustrates how the lossy material is applied to the filter. Two 1.5 mm gaps are cut into the picture frame lossy material to avoid degrading the differential signal. The thickness of the lossy material is about 0.7 mm. Figure 4.6 shows the lossy material has a negligible effect on the differential signal and a very small impact on the primary resonance of the common mode signal. But for the TRP results comparison shown in Figure 4.5, about 6 dB reduction can be observed at 11 GHz when one layer of lossy material is applied. In addition, about 5 dB more reduction is achieved when using two layers of lossy material. The TRP was unaffected below 10 GHz because the plane resonance was not a dominant radiation mechanism at those frequencies.

The second method to reduce the TRP impact of the filter is to put the filter into a shielded enclosure. Most printed circuit boards with high-speed differential interfaces are placed inside shielded enclosures, so this method is very relevant for practical applications.

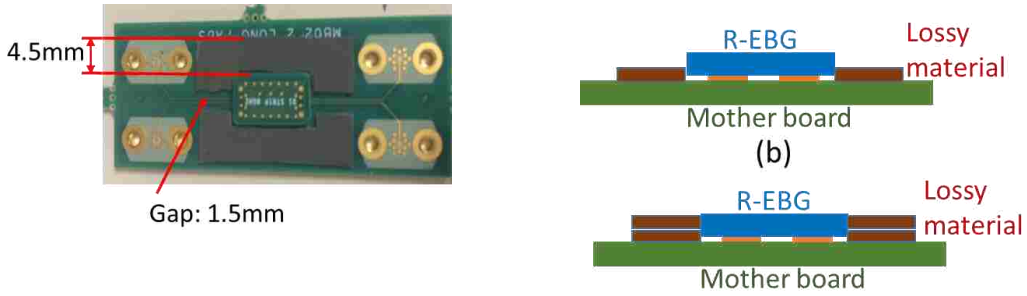

(a) (b)

Figure 4.4. Picture frame of lossy material on the removable EBG board: (a) one layer of lossy material and (b) two layers of lossy material.

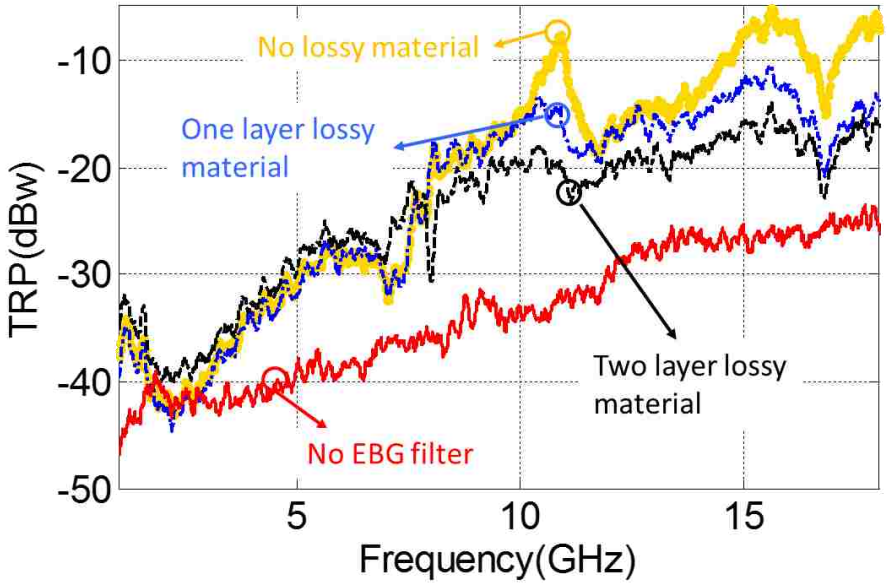

Figure 4.5. Measured TRP results comparison for lossy material.

In Figure 4.7 (a)-(b), the removable EBG board (or reference board for the control case) and the power splitter were put inside a metal box. Two ports of the filter were connected with the output of the splitter and the other two ports of the filter are connected to the two output ports of the shielded enclosure. For completeness, the case without the shielding box is included in the measurement setup shown in Figure 4.7 (c). In those

tests, two 60 inch coaxial cables were connected to the output ports of the box, which are left open at the termination end.

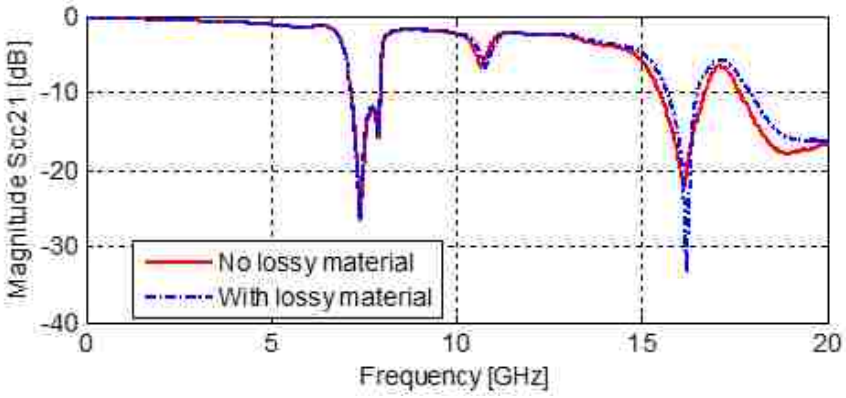

(a)

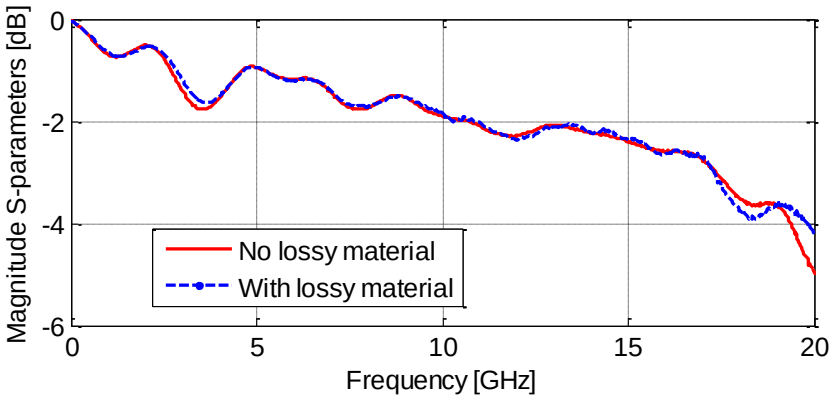

(b)

Figure 4.6. S-parameter (before de-embedding) comparison--with 2 layers of material vs. without lossy material: (a) $S_{cc}21$ and (b)$S_{dd}21$.

Figure 4.8 shows the TRP measurement results taken in the reverberation chamber. The case with the filter has higher radiated power than the reference board, which is the same behavior shown in Figure 4.5. But, when we place both cases inside a shielded enclosure, the TRP is reduced to roughly the same level. This shows that traditional shielding is effective at containing increased TRP from the removable EBG filter. Most importantly, when the shielding box is used, the TRP of the filter board is

about 14 dB lower than the reference board over the working frequency range of the filter. The TRP is lower because the CM currents are significantly attenuated before the signals exit the shielding box and enter the cable. Finally, we observe that no additional radiation was introduced at other frequencies.

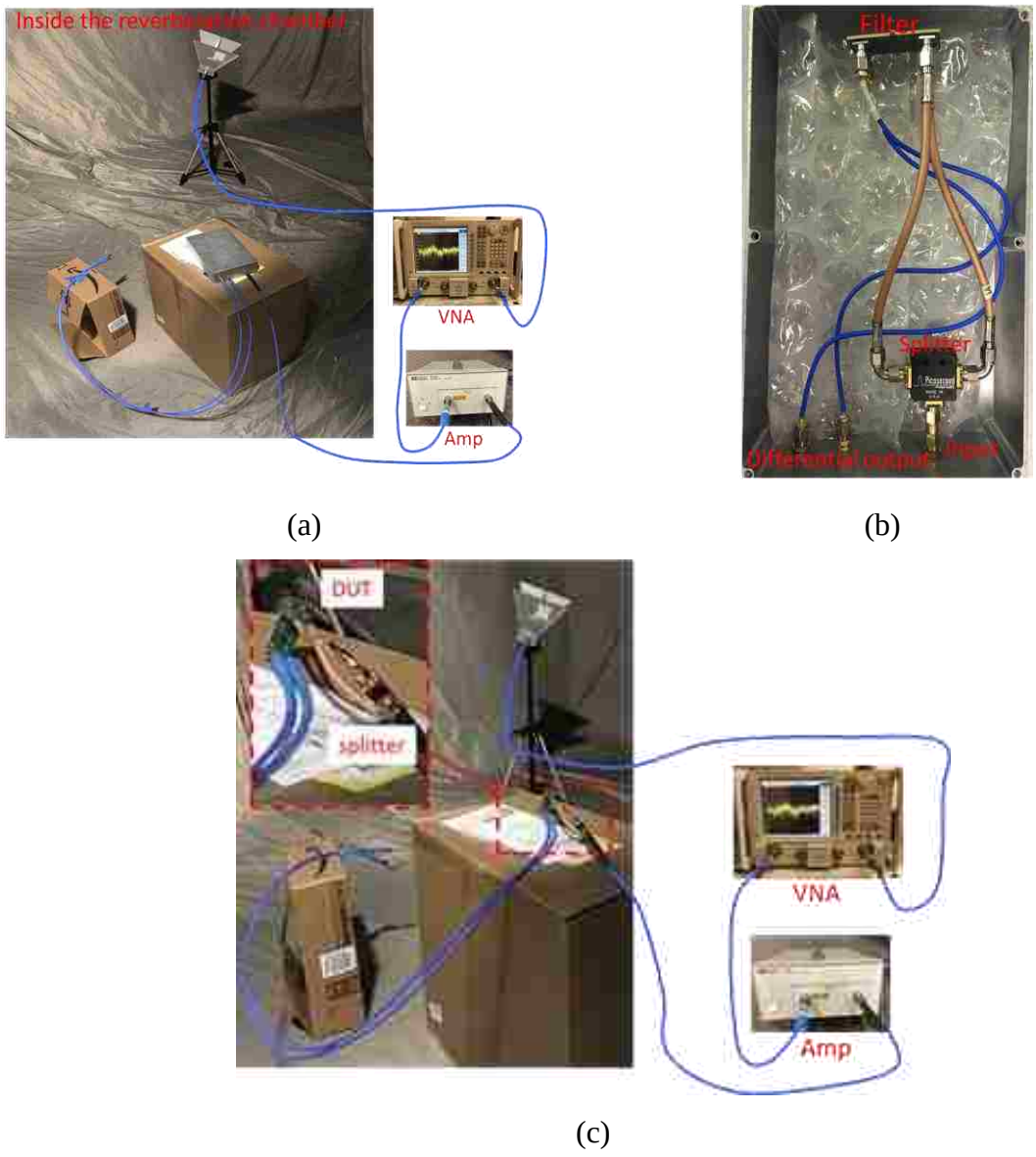

(a) (b)

(c)

Figure 4.7. Experiment setup for measuring the total radiated power: (a) measurement setup with the shielding box (b) removable EBG filter and splitter inside the shielding box, (c) measurement setup without the shielding box.

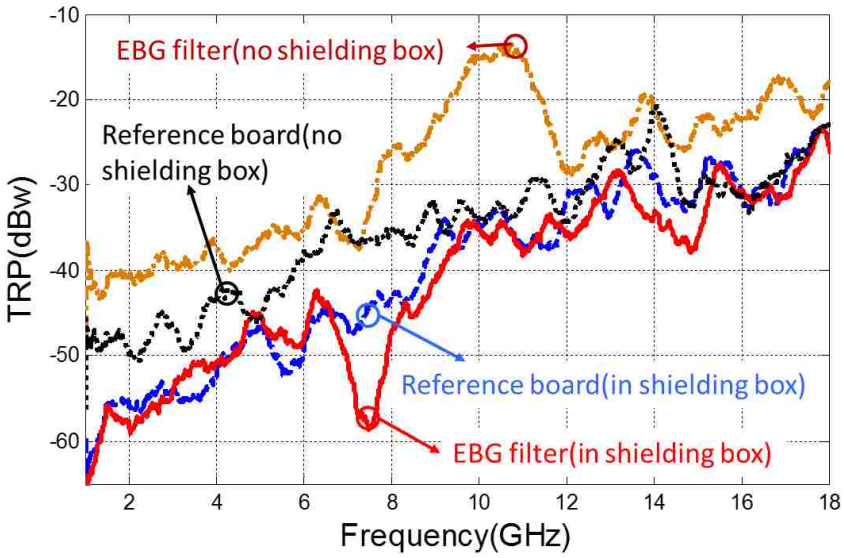

Figure 4.8. Measured TRP results comparison between a reference board and a removable RBG filter.

5. CONCLUSION

A removable “sandwich” EBG-based common mode filter was designed, manufactured, and tested in this paper. The advantages of this filter are numerous. It can be installed, substituted and removed by the typical soldering assembly process, which is easy to meet the filter needs of PCB differential link designers at any stage of the design process. The device is a viable answer to the presence of unexpected common mode noise and even the changing of data rates on particular lines which would require filtering at different target frequencies. The external dimensions of the removable filter remain unchanged in order to fit the fixed filter area allocated on the board. The total radiated power of the removable filter component was studied, and we found that TRP increases when the filter is used. Two methods are discussed to reduce the added TRP. One way is to add picture-frame-shaped lossy material around this filter to suppress the unwanted TRP without affecting the differential signals. Another is to put the filter inside a shielded enclosure, which prevents the increased TRP of the filter from radiating outside the box and reduces the system-level emissions due to the cable or its attachment to the enclosure by suppressing the common mode currents over the designed filter bandwidth. For shielded systems with radiated emissions issues being driven by the common mode currents on cables, backshells, or cable housings, this removable EBG-based filter can be an effective remedy.

REFERENCES

[1] S. Shahparnia and O. M. Ramahi, "Electromagnetic interference (EMI) reduction from printed circuit boards (PCB) using electromagnetic bandgap structures," in IEEE Trans. Electromagn. Compat., vol. 46, no. 4, pp. 580–587, Nov. 2004.

[2] B. Archambeault, S. Connor, and J. Diepenbrock, "EMI emissions from mismatch in high-speed *differential* signal trace and cables," in Proc. IEEE Int. Symp. Electromagn. Compat., Hawaii, Jul. 2007, pp. 1-6.

[3] G. Li, W. Qian, A. Radchenko, G. Hess, R. Hoeckele, P. Jalbert, T. Van Doren, D. Pommerenke, and D. Beetner, "Estimating the radiated emissions from cables attached to a switching power supply in a MIL-STD 461 test," in IEEE Int. Symp. EMC, Denver, CO, pp. 626-631, 2013.

[4] Z. Yan; Y. Xiong; W. Yu; Y. Wang, "An Improved Miniaturized Three-Layer *Embedded* Electromagnetic Bandgap Structure," in IEEE Trans. Antennas Propag, pp. 2832-2837, May 2014.

[5] G.-H. Shiue, C.-L. Hsu, C.-L. Yeh, and C.-F. Hsu, "A comprehensive investigation of a *common*-mode filter for gigahertz differential signals using quarter-wavelength resonators", in IEEE Trans. Compon., Packag., Manuf. Technol., vol. 4, no. 1, pp. 134–144, Jan. 2014.

[6] Q. Liu; G. Li.; V. Khilkevich; D. Pommerenke, "Common-Mode Filters With *Interdigital* Fingers for Harmonics Suppression and Lossy Materials for Broadband Suppression," in IEEE Trans. Electromagn. Compat., vol.57, no.6, pp.1740-1743, Dec. 2015.

[7] S. Wu.; C. Tsai; T. Wu; T. Itoh, "A Novel Wideband Common-Mode Suppression Filter for Gigahertz Differential Signals Using Coupled Patterned Ground Structure," in Microwave Theory and Techniques, IEEE Trans. on , vol.57, no.4, pp.848,855, Apr. 2009.

[8] F.de Paulis, A. Orlandi, "Signal Integrity Analysis of Single-Ended and Differential Striplines in Presence of EBG Planar Structures", in IEEE Microwave and Wireless Components Letters, vol. 19, nr. 9, Sep. 2009.

[9] F. De Paulis, L. Raimondo, D. Di Febo, B. Archambeault, S. Connor, A. Orlandi, "Experimental Validation of Common-Mode Filtering Performances of Planar Electromagnetic Band-gap Structures", in Proc. of 2010 IEEE Symposium on Electromagnetic Compatibility, Fort Lauderdale, FL, USA, 25-30 Jul. 2010.

[10] F. De Paulis, L. Raimondo, S. Connor, B. Archambeault, A. Orlandi, "Design of a Common Mode Filter by using Planar Electromagnetic Bandgap Structures", in IEEE Trans. on Advanced Packaging, vol. 33, n. 44, Nov. 2010.

[11] F. De Paulis, L. Raimondo, D. Di Febo, A. Orlandi, "Trace Routing Strategies for Improving Common Mode Filter Performances in High Speed Digital Differential Interconnects", in Proc. of 15th IEEE Workshop on Signal Propagation on Interconnects, Naples, Italy, May 08-11, 2011.

[12] F. De Paulis, L. Raimondo, S. Connor, B. Archambeault, A. Orlandi, "Compact Configuration for Common Mode Filter Design based on Planar Electromagnetic Bandgap Structures", in IEEE Trans. on Electromagn. Compat. vol. 54, no. 3, pp. 646-655, June 2012.

[13] F. de Paulis, B. Archambeault, M. H. Nisanci, S. Connor, and A. Orlandi, "Miniaturization of Common Mode Filter Based on EBG Patch Resonance", in Proc. IEC DesignCon 2012, January 30-February 2, 2012, Santa Clara, USA.

[14] M.H. Nisanci, F.De Paulis, A.Orlandi, B. Archambeault, S.Connor, "Optimum Geometrical parameters for the EBG-Based Common Mode Filter Design", in Proc. of 2012 IEEE Symposium on Electromagn. Compat., Pittsburgh, PA, USA, 5-10 August, 2012.

[15] X. Gu, R. Rimolo-Donadio, Y. Kwark, C. Baks, F. de Paulis, M. H. Nisanci, A. Orlandi, B. Archambeault, S. Connor, Design and "Experimental Validation of Compact Common Mode Filter Based on EBG Technology", in Proc. of IEC DesignCon 2013, January 28-31, 2013, Santa Clara, USA.

[16] F. de Paulis, M. H. Nisanci, A. Orlandi, X. Gu, R. Rimolo-Donadio, Y. Kwark, C. Baks, B. Archambeault, S. Connor, "Experimental Validation of an 8 GHz EBG Based Common Mode Filter and Impact on Manufacturing Uncertainties", in Proc. of IEEE Int. Symp. on EMC, August 5-9, 2013, Denver, CO, USA.

[17] C. Olivieri, F. de Paulis, A. Orlandi, S. Connor, B. Archambeault, "Miniaturization Approach for EBG-Based Common Mode Filter and Interference Analysis", IEEE Int. Symp. on EMC, March 15-20, 2015, Santa Clara CA, USA.

[18] F. de Paulis, M. Cracraft, D.Di Febo, H.M.Nisanci, S. Connor, B. Archambeault, A. Orlandi, "EBG-based common mode microstrip and stripline filters: experimental investigation of performances and crosstalk", IEEE Trans. on Electromagn. Compat., early access article, May 2015.

[19] F. de Paulis, M. Cracraft, C. Olivieri, S. Connor, A. Orlandi, B. Archambeault, "EBG-Based Common Mode Stripline Filters: Experimental Investigation on Interlayer Crosstalk", IEEE Trans. on Electromagn. Compat., vol. 57, nr. 6, pp. 1416-1424, Dec. 2015.

[20] M.A. Varner, F. de Paulis, A. Orlandi, S. Connor, M. Cracraft, B. Archambeault, H.Nisanci, D. di Febo, "Removable EBG-Based Common Mode Filter for High Speed Signaling: Design and Experimental Validation", IEEE Trans. on Electromagn. Compat., Special Issue on the 2014 IEEE International Symposium on EMC, vol. 57, nr. 4, pp. 672-679, Aug. 2015.

[21] L. Raimondo, F. De Paulis, A. Orlandi, "A Simple and Efficient Design Procedure for Planar Electromagnetic Band-gap Structures on Printed Circuit Boards", IEEE Trans. on Electromagn. Compat., Vol. 53, nr. 2, pp. 482-490, May 2011.

[22] F. De Paulis and A. Orlandi, "Accurate and efficient analysis of planar electromagnetic band-gap structures for power bus noise mitigation in the GHz band", in Proc. of Electromagnetics Research B, Vol. 37, 59-80, 2012.

[23] Computer Simulation Technology, CST STudiuo Suite 2015, www.cst.com.

[24] X. Ye; J. Fan; B. Chen; J. Drewniak, Q. Chen, "Accurate characterization of PCB transmission lines for high speed interconnect," Electromagn. Compat.(APEMC), 2015 Asia-Pacific Symp. on , vol., no., pp.16-19, 26-29 May 2015.

II. COMMON-MODE FILTERS WITH INTERDIGITAL FINGERS FOR HARMONICS SUPPRESSION AND LOSSY MATERIALS FOR BROADBAND SUPPRESSION

Qian Liu, *Student Member, IEEE*, Guanghua Li, *Student Member, IEEE*, Victor Khilkevich, *Member, IEEE*, David Pommerenke, *Fellow, IEEE*

ABSTRACT

Common-mode (CM) noise on differentialmicrostrip lines can be suppressed by PCB-embedded filters. These filters use resonating or broadband structures such that only the field from the CM signal couples to them. Based on a quarter-wavelength resonator, a new PCB filter is designed having an electrical size of only $0.15\ \lambda \times 0.065\ \lambda$, where λ is the effective wavelength in the CM filter. Its interdigital structure is also capable of suppressing higher order harmonics of the CM signal and can be used for USB 3.0 to mitigate electromagnetic interference. Further, a novel broadband suppression structure is described that uses magnetically lossy material to suppress the CM signal from 4.6 to 20 GHz without strongly affecting the intended differential signal.

Index Terms— Broadband filter, common-mode filter, differential signal, quarter-wavelength, narrowband filter.

1. INTRODUCTION

Common mode (CM) noise is caused by an imbalanced differential signal path, which in turn causes electromagnetic interference problems [1]. These problems can be mitigated by suppressing the CM noise using CM filters embedded in the signal path. These filters have been widely designed and analyzed using defected ground structures (DGS) and electromagnetic bandgap (EBG) structures [2]–[5]. The 0.4 $\lambda \times 0.16\ \lambda$ (0.064 λ^2) (where λ is the effective wavelength in the CM filter) size of the EBG structure was achieved by removing a central patch in a 5-layer stackup [3]. The dimensions were further decreased to 0.21 $\lambda \times 0.21\ \lambda$ (0.044 λ^2) by introducing a C-shaped patterned ground structure found in [6] and decreased to 0.026 λ^2 by using coupled synthesized microstrip line and modified mushroom resonators as found in [7]. Furthermore, a quarter-wavelength resonator was used in the filter design (electrical size 0.01 $\lambda \times 0.25\ \lambda$=0.0025 λ^2) in [8] for an even smaller dimension compared to DGS and EBG structures.

According to the suppression bandwidth, the CM filter can be subdivided into narrowband and broadband filters. The narrow- band filter suppresses signals around a single frequency (and maybe its harmonics). The wideband filter has a much broader stopband, which can be achieved by combining several narrow- band filters, but at the expense of occupied area. High-speed digital signals often contain harmonics of the clock frequency. So a compact CM filter that can suppress a single frequency as well as the harmonics of that frequency is desirable.

In order to further decrease the filter's dimension, this paper introduces a CM filter with an electrical size of only 0.15 $\lambda \times 0.065\ \lambda$ (0.0098 λ^2), based on an interdigital quarter-wavelength resonator. This filter has the additional advantage of suppressing CM noise at both the odd and even harmonic frequencies of the resonator. Additionally, this paper discusses a new way to suppress broadband CM noise up to 20 GHz by overlaying magnetically lossy material on a metal patch above a PCB-based filter.

2. NARROWBAND CM SUPRESSION FILTER

A quarter-wavelength resonator-based filter, as shown in Figure 2.1, suppresses CM noise in a differential signal path [8]. The resonator is located between the differential signal traces on the top layer and a ground plane on the third layer of a printed circuit board (PCB). One end of the resonator is terminated through a via to the ground plane, while the other end is left open in the substrate. Because of this resonator, the CM noise along the signal path is attenuated, while the differential mode (DM) signals are distorted by 4 dB at frequency below 10 GHz by the filter [8].

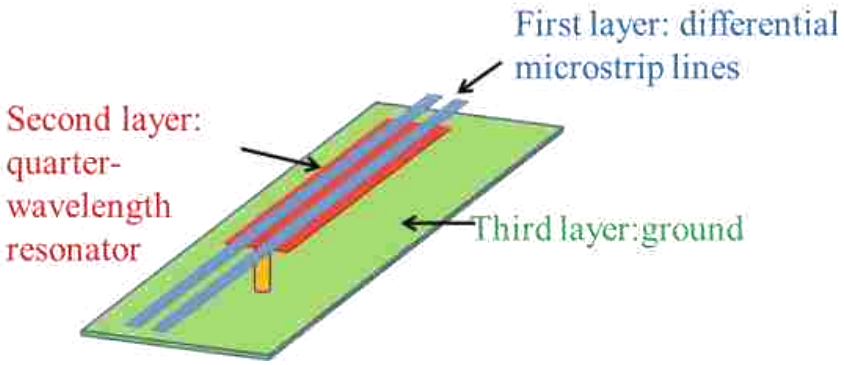

Figure 2.1. Structure of a CM filter based on a quarter-wavelength resonator.

The filter suppresses only the CM noise around the odd harmonics of the resonator, but transmits the noise around the even harmonics. In order to suppress the noise at both odd and even harmonic frequencies, an interdigital resonator based on this CM filter was designed with dimensions shown in Figure 2.2[9]. The interdigital fingers increase the capacitance from the resonator to the ground plane; thus, decreasing the electric size of the resonator. The filter was built using a three-layer PCB ($\text{Ɛ}r \approx 3.7$ and $\tan\delta \approx 0.077$) with a fabricated sample shown in the lower right of Figure 2.3.

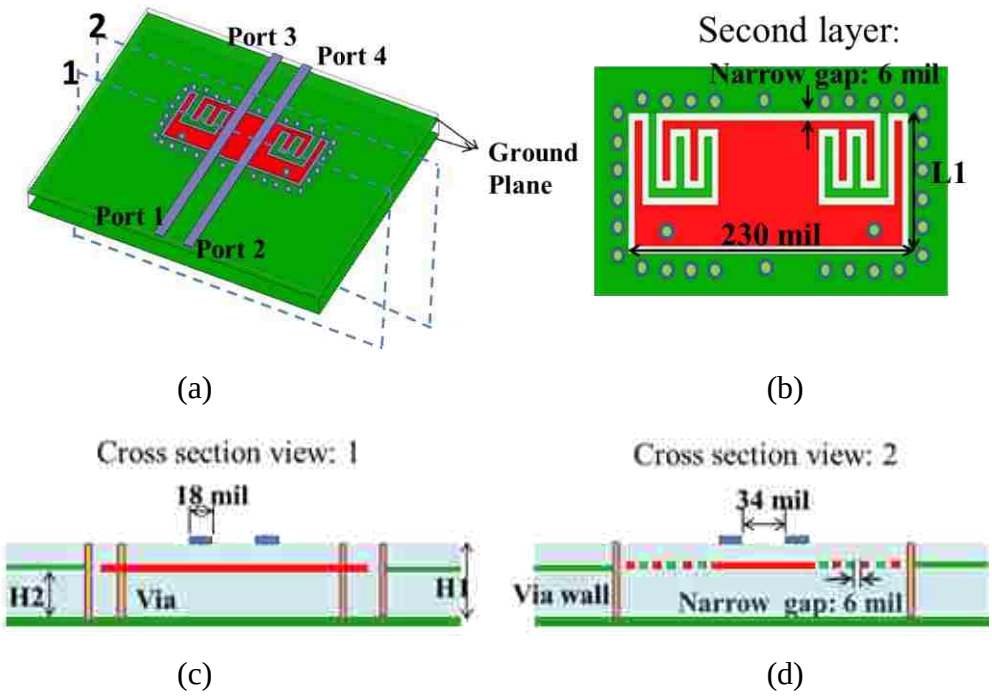

Figure 2.2. Proposed CM suppression filter: (a) isometric view, (b) top view of the structure on layer 2, (c) cross-sectional view 1, and (d) cross-sectional view 2.

Figure 2.3 shows a comparison of the simulated and measured insertion loss up to 20 GHz for the fabricated CM suppression filter. A series of CM stopbands was observed at harmonics of 5 GHz. Meanwhile, differential signals were minimally affected by the filter. Note that the electrical size of the proposed structure was only 0.15 $\lambda \times 0.065\ \lambda$ ($0.0098\ \lambda^2$). This electrically small size was achieved by the parasitic capacitance in the interdigital stubs shown in the dashed boxes in Figure 2.4(a). The filter's current distribution is complex and it is not easy to associate the higher resonances with individual features. However, the nature of the 5-GHz resonance can be explained as a capacitive loaded quarter-wavelength resonator. Removing the outer fingers [shown in Figure 2.4(a)] yields a modified resonator [see Figure 2.4(b)]. The effect of the outer finger on the resonant frequency is shown in Figure 2.5. The first resonance is not affected. For higher resonances, the via structure no longer offers a short because the outer finger also influences the resonances.

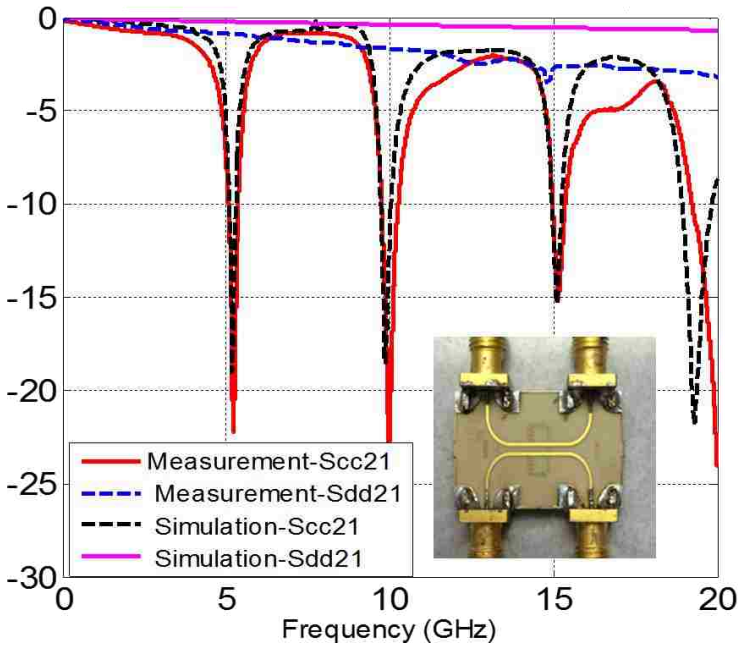

Figure 2.3. Simulated and measured differential insertion loss $|S_{dd}|$ and $|S_{cc}|$ for the proposed CM suppression filter with interdigital stubs.

Manufacturing variations and unknown dielectric properties lead to variations in the stopband frequencies. A set of varia- tions of the structure was studied. As an example, the effect of the total lateral length L1 from Figure 2.2 on the stopband frequencies is shown in Figure 2.6. The measurement results are further summarized in Table 2.1 and Table 2.2 for reference.

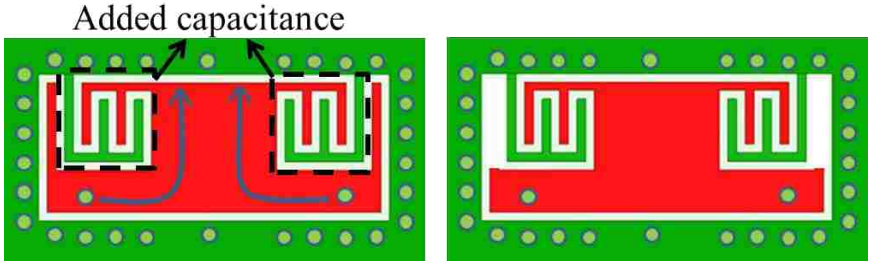

(a) (b)

Figure 2.4. Top view of the structure on layer 2: (a) whole structure and (b) modified resonator (without the outer finger).

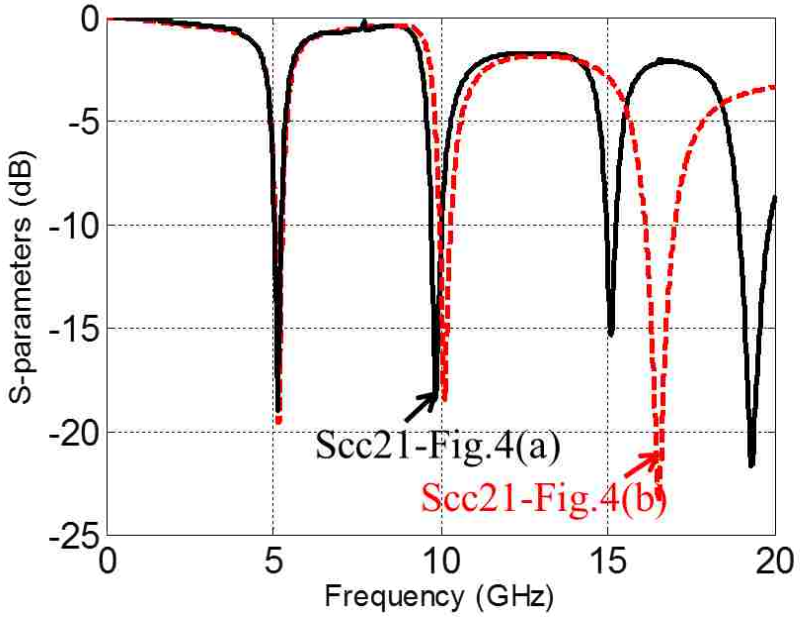

Figure 2.5. Comparison of the simulated results of the structures in Figure 2.4.

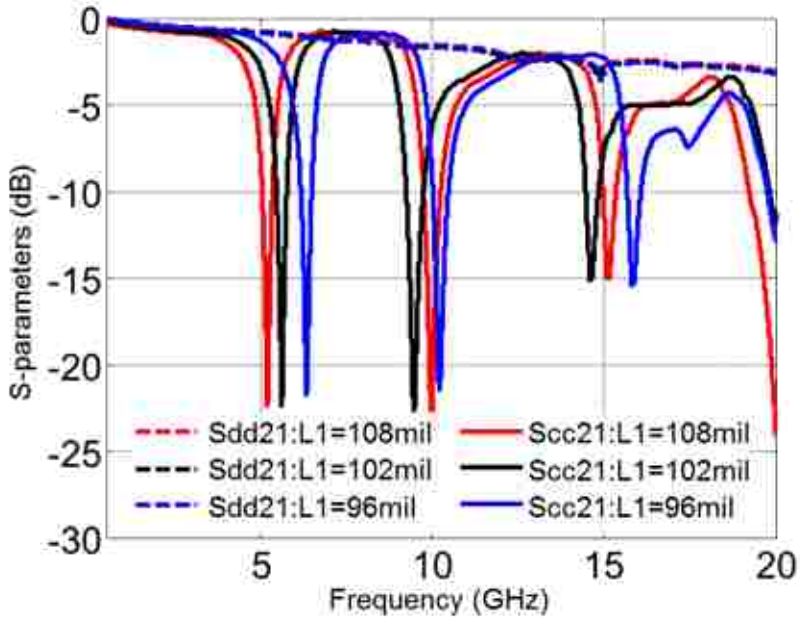

Figure 2.6. Effect of interdigital stub length L1 on the center frequency of the CM suppression filter.

Scaling in total lateral length L1 direction (Figure 2.2) provides an opportunity to design a CM filter at different frequencies. For example, by changing the total lateral length L1 from 108 mils to 88 mils one can move the target frequency from 5 to 6 GHz, as shown in Figure 2.7. Table 2.2 lists the comparison of the electrical size between filters designed for operating at 5GHz and 6GHz. The final tuning of the filter is achieved by scaling the total lateral length L1 and using numerical optimization of full wave simulations to determine other geometrical parameters of the structure.

Table 2.1. Suppression of CM Signal.

L1	5 GHz	10 GHz	15 GHz
108mils	8.9dB	21.6dB	11.4dB
102mils	3.4dB	6.4dB	7.6dB
96mils	1.4dB	9.9dB	2.4dB

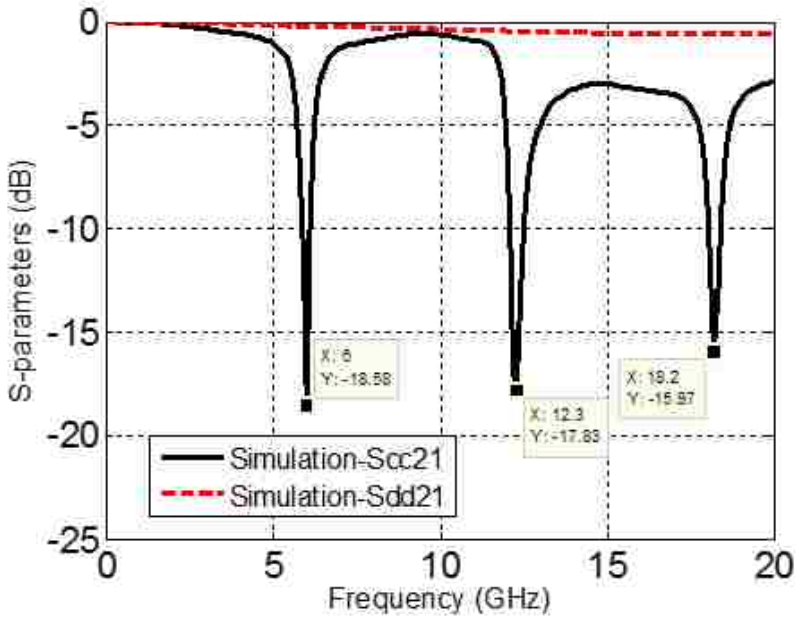

Figure 2.7. Simulated differential insertion loss |Sdd | and |Scc | for the proposed CM suppression filter operating at 6 GHz.

Table 2.2. Comparison of target frequency and electrical size.

First resonant frequency	Electrical length
5 GHz	0.15 λ × 0.065 λ
6 GHz	0.17 λ × 0.063 λ

3. BROADBAND CM SUPPRESSION FILTER

The CM suppression filter in Section II suffers from the draw- back of only suppressing CM noise in narrow frequency bands, which may be insufficient to ensure signal quality for a signal path under the influence of broadband noise. This issue can be solved by cascading several narrowband filters with differ- ent stopband frequencies, but at the cost of increased size on the PCB. Another method is to dissipate the CM energy in the signal path with broadband lossy materials, such that the broadband CM noise cannot propagate along the path efficiently. Mean- while, the energy of the DM signals is only slightly absorbed by the lossy materials.

The broadband CM suppression filter described in this section utilizes a PCB with overlaid magnetically lossy material and is illustrated in Figure 3.1. A thin copper patch was placed above the differential trace and the lossy material was placed directly above this conductor. According to the conceptual field distributions illustrated in Figure 3.1, fields from the CM current will penetrate the lossy material, while the fields from the DM current will be contained underneath the patch. This field be- havior was further validated by the simulated field distributions with and without the additional copper patch for both DM and CM excitations. These results suggest that lossy material placed above the patch will significantly affect the CM noise, but not the DM signals.

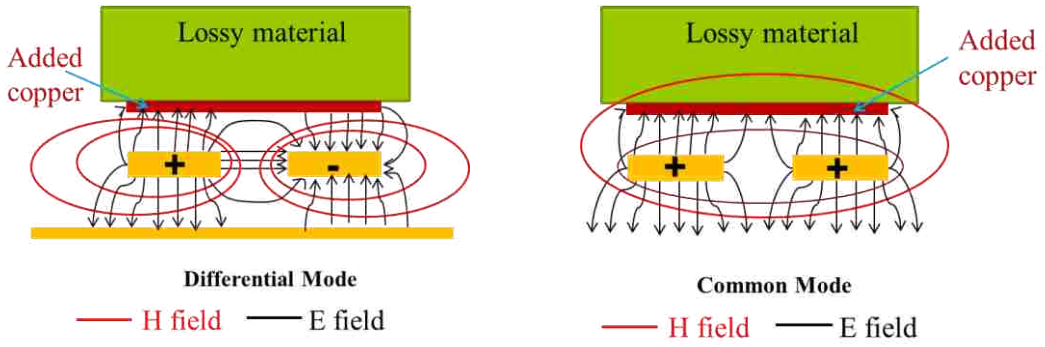

(a) (b)

Figure 3.1. Conceptual field distribution from: (a) DM signal and (b) CM noise in a differential trace with overlaid metal and additional lossy material.

The field distribution shown in Figure 3.2 depends highly on the distance of the patch above the differential trace. If the metal is placed too close to the trace, it will strongly affect the field distribution and, therefore, the DM impedance leading to reflections. This is illustrated by the significant ripples in |Sdd21 | in Figure 3.4 and by the eye diagram in Figure 3.5 (b) for the distance of 1 mil. The eye diagram shown in Figure 3.5(a) is used as a reference for comparison. On the other hand, if the metal is placed too far away from the trace, the additional lossy material does not interact strongly with the field from the CM current in the trace, and the CM noise will not be significantly attenuated, as indicated by the |Scc21 | in Figure 3.4. Distances from 1 to 15 mil were simulated in 1 mil increments, and it was found that a distance of 3 mils provides the best performance. The goal of these simulations was simultaneous achieving smooth roll-off of |Sdd21 | and a low value of |Scc21 |, as shown in Figure 3.4. The corresponding eye diagram is shown in Figure 3.5. (c).

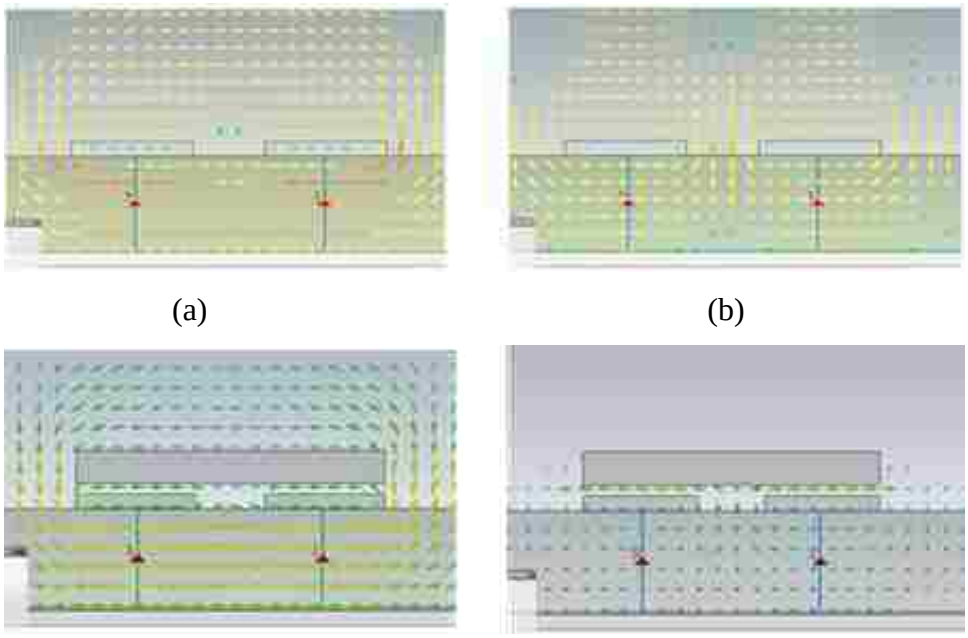

Figure 3.2. Simulated H-field distribution around a differential trace generated by: (a) CM noise, (b) DM signal, (c) CM noise, with a conductor placed above the trace, and (d) DM signal with a conductor placed above the trace.

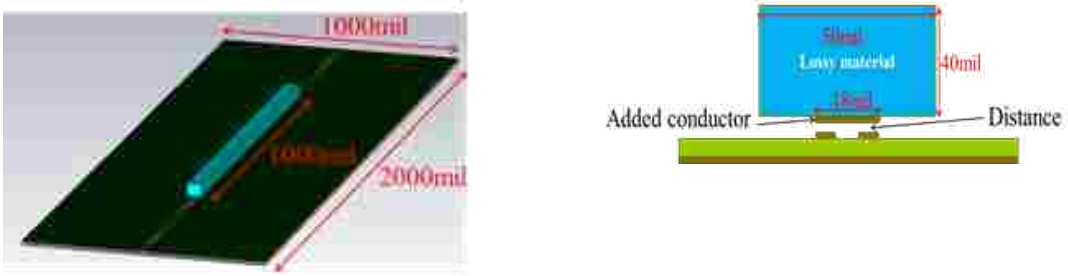

(a) (b)

Figure 3.3. Proposed broadband CM suppression filter: (a) 3D view (b) cross section view.

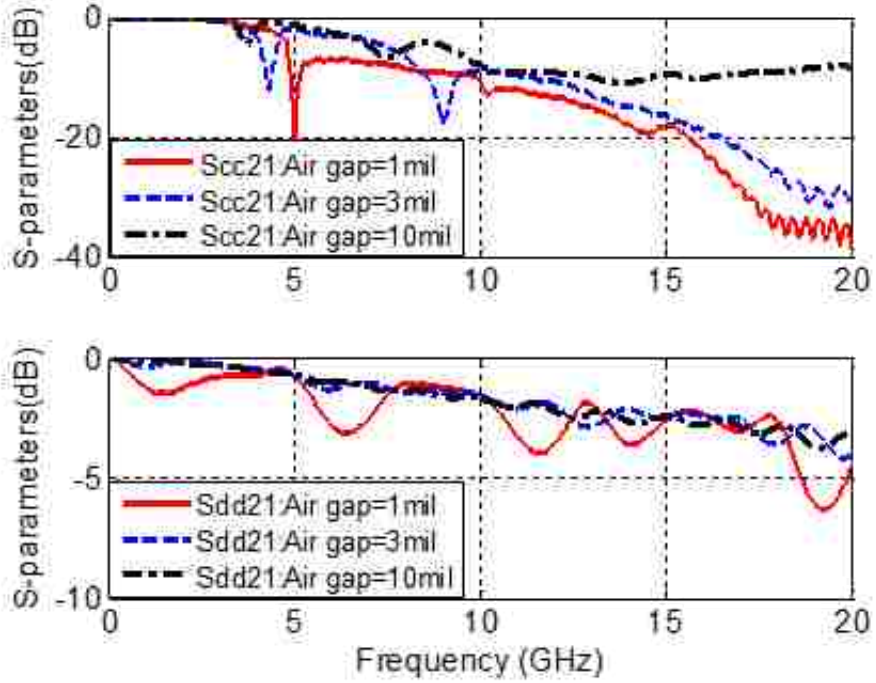

Figure 3.4. Effect on insertion loss |Scc21 | and |Sdd21 | as a function of the distance between the added conductor and the differential trace.

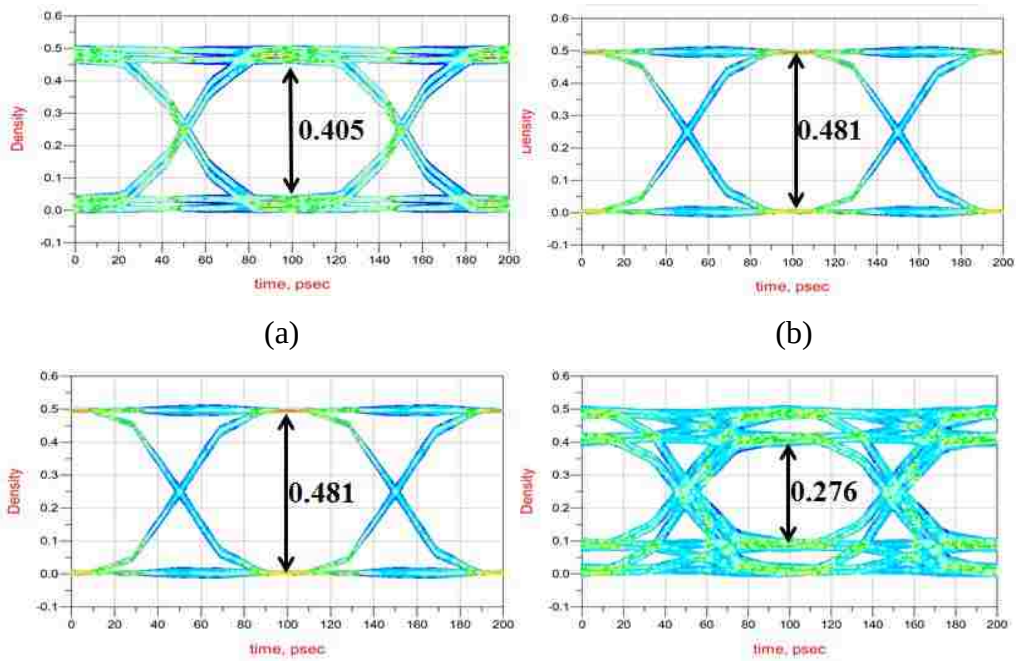

(a) (b)

(c) (d)

Figure 3.5. Simulated eye diagrams of a differential trace: (a) without the overly- ing metal and the additional lossy material as a reference, and with the overlying metal and the additional lossy material for a distance of (b) 1 mil, (c) 3 mils, and (d) 10 mils.

4. COMBINED CM SUPPRESSION FILTER

The bandwidth of the proprietary lossy material-based filter in Section III is limited partly by the bandwidth of the over- lying lossy material ($\varepsilon_r \approx 17$ and $\tan \delta_\varepsilon \approx 0.004$; μ_r 1.2 and $\tan \delta_\mu \approx 1$ at 10 GHz). The lossy material cannot help suppress CM noise at frequencies below the material usable frequency. For example, the magnitude of $|S_{cc}21|$ is greater than –5 dB from 5 to 8 GHz (as shown in Figure 3.4.). One can suppress the CM noise in this frequency range by combining a quarter- wavelength resonator-based filter with the lossy material-based filter in Section III, leading to an even broader bandwidth.

The A quarter-wavelength resonator-based filter, shown in Figure 4.1, was built using the same setup as in Figure 2.2. The resonator had two open-ended stubs sharing two vias terminated to the ground plane. The 196-mils-long stub created a stop band at 5.2 GHz, while the 205-mils-long stub created a second stop- band at 4.8 GHz. The simulation and measurement results are shown in Figure 4.2. As expected, this filter cannot suppress CM noise at frequencies between 8 and 16 GHz.

A piece of 1000-mils-long and 50-mils-wide proprietary magnetic-lossy material was placed 3.4 mils above the quarter- wavelength resonator-based filter, shown in the bottom right of Figure 4.3., using the same method of placement as described in the previous section. A 3.4-mil-thick paper masking tape was used as a spacer to sustain between the lossy material and the filter. Both simulated and measured results shown in Figure 4.3 indicate a smaller $|S_{cc}21|$ than that shown in Figure 3.4, while keeping $|S_{dd}21|$ below –7 dB up to 20 GHz. This validated the method of combining different structures for broadening the filter bandwidth.

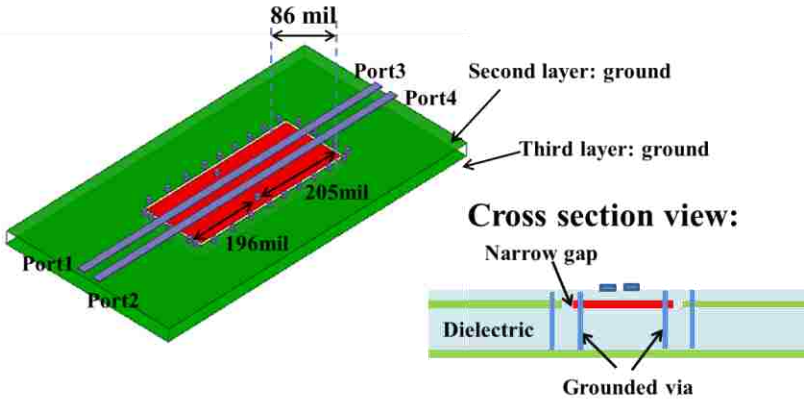

(a) (b)

Figure 4.1. Geometry of a resonator as a basis for overlaying lossy material for a broadband CM suppression filter: (a) isometric view and (b) cross section view.

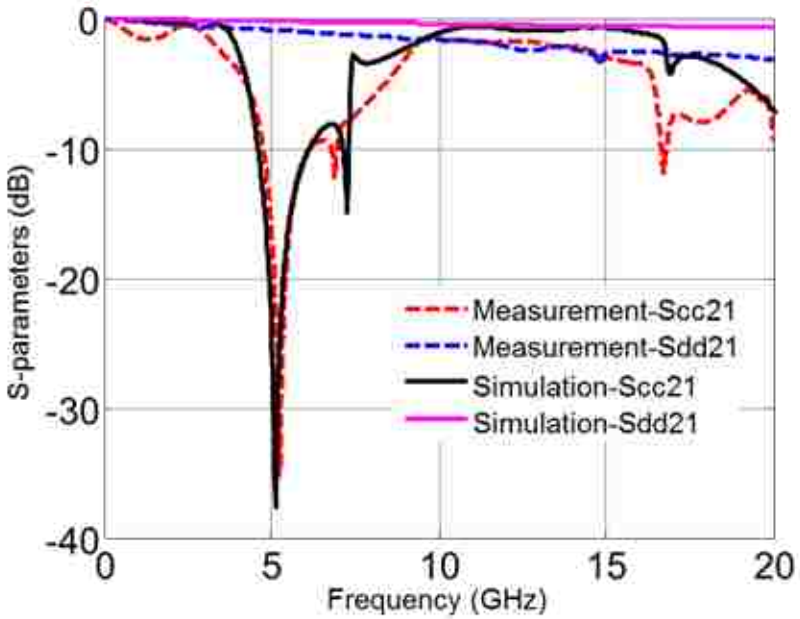

Figure 4.2. Simulated and measured data comparison for the structure in Figure 4.1.

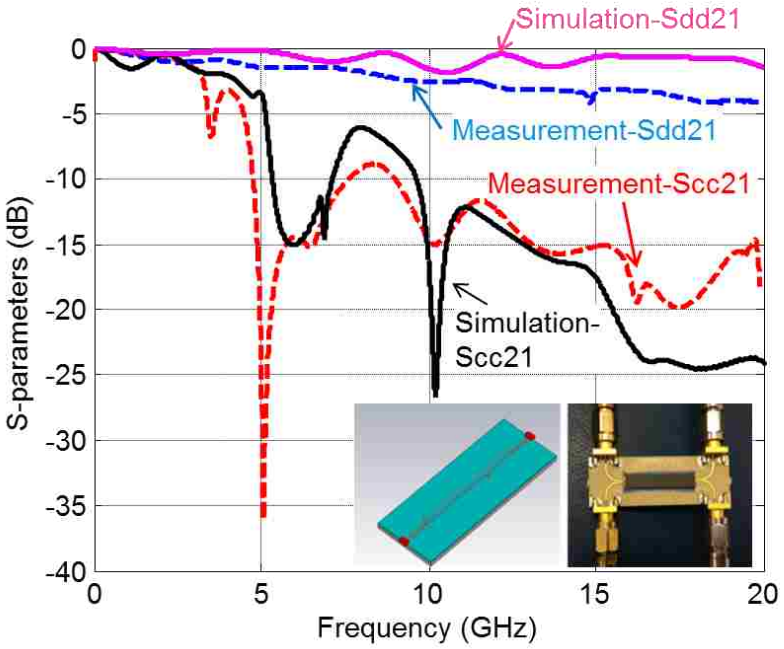

Figure 4.3. Simulated and measured data comparison of combined structures.

5. CONCLUSION

A narrowband CM suppression filter based on an inter-digital resonator with electrical area as small as $0.0098\ \lambda^2$ was designed. The filter is able to suppress CM noise at both odd and even harmonics of the fundamental resonance frequency. Additionally, a broadband CM filter capable of effectively suppressing broadband noise in the frequency range from 4.6 GHz to 20 GHz was constructed by overlaying lossy materials on a piece of metal placed above a quarter-wavelength resonator.

REFERENCES

[1] B. Archambeault, S. Connor, and J. Diepenbrock, “EMI emissions from mismatch in high-speed differential signal trace and cables,” in Proc. IEEE Int. Symp. Trans. Electromagn. Compat., Hawaii, Jul. 2007, pp. 1-6.

[2] Z. Yan; Y. Xiong; W. Yu; Y. Wang, "An Improved Miniaturized Three-Layer Embedded Electromagnetic Bandgap Structure," IEEE Trans. Antennas Propag, pp. 2832-2837, May 2014.

[3] C. Olivieri, F. de Paulis, S. Connor, B. Archambeault, and A. Orlandi, "Miniaturization approach for EBG-based common mode filter and interference analysis," IEEE Symp. EMC, Santa Clara,CA, pp. 91-96, March. 2015.

[4] Y. Pang, Z. Feng, "A compact common-mode filter for GHz differential signals using defected ground structure and shorted microstrip stubs," 2012 Int. Conference, Microw. and Millimeter Wave Technology , May 2012, pp. 1-4.

[5] W. Liu; C. Tsai, T. Han, and T. Wu, "An Embedded Common-Mode Suppression Filter for GHz Differential Signals Using Periodic Defected Ground Plane," IEEE Trans. Microw. Wireless Compon. Lett., pp. 248-250, Apr. 2008.

[6] T. Weng, C. Tsai, C. Chen, D. Han and T. Wu, "Synthesis Model and Design of a Common-Mode Bandstop Filter (CM-BSF) With an All-Pass Characteristic for High-Speed Differential Signals," IEEE Trans. Microw. Theory Tech, Aug. 2014.

[7] B. Su; T. Ma, "Miniaturized Common-Mode Filter Using Coupled Synthesized Lines and Mushroom Resonators for High-Speed Differential Signals," IEEE Trans. Microw. Wireless Compon. Lett., vol.25, no.2, pp.112,114, Feb. 2015.

[8] G. Shiue, C Hsu, C. Yeh, and C. Hsu, "A Comprehensive Investigation of a Common-Mode Filter for Gigahertz Differential Signals Using Quarter-Wavelength Resonators," IEEE Trans. Compon., Packag.,Manuf. Technol, vol. 4, no. 1, pp. 134–144, Jan. 2014.

[9] Q. Liu, S. Xu, and D. Pommerenke, "PCB structures for common mode suppression on differential microstrip lines," in IEEE Int. Symp. *EMC*, Raleigh, NC, Aug. 2014, pp.533-537.

III. PCB STRUCTURE FOR COMMON MODE SUPPRESSION ON DIFFEREITNAIL MICROSTRIP LINES

Qian Liu, Student Member, IEEE, Shuai Xu, Member, IEEE, David Pommerenke, Fellow, IEEE

ABSTRACT

Common mode noise on differential microstrip lines can be suppressed by PCB embedded filters. These filters are basically resonators, and only the common mode signal can couple to them. Though such structure suppress common mode signal only in narrow bands because of the resonant nature, they can be combined to produce broadband filtering effect. The dimension of such filters could be further reduced by adding lumped elements. In this paper, design principles of the PCB filters are given, and examples are given to demonstrate these rules. At last, a new PCB filter structure is proposed with an electrical size of only $0.04\lambda \times 0.067\lambda$ which is capable of suppressing the higher order harmonics of common mode signal.

Index Terms— Common mode filter, differential signal, quarter-wavelength, lower resonant frequency.

1. INTRODUCTION

All differential interfaces will carry common mode signals. Common mode signals could originate from drivers, non-identical rise and fall times, unbalanced traces or skew, etc. Common mode signals may couple to structures capable of radiation, such as the outside of cable shields and enclosures, causing EMI problems. These problems can be solved by improving the driver, removing the structures that cause differential to common mode conversion, filtering the common mode current, or reducing the coupling to structures capable of radiating the signal. This paper focuses on structures that filter common mode currents on differential traces.

Common mode suppression on differential signals can be subdivided into four classes: active compensation of common mode, which is more suitable for lower frequencies; common mode compensation structures; discrete components for suppression, such as common mode chokes; and common mode suppression structures, integrated into printed circuit boards (PCBs). An example of common mode compensation structures is bended differential lines using compensation capacitors [1] and/or inductors [2] so as to improve the symmetry of the differential pairs. The third class of filters is discrete component such as common mode chokes. A common mode choke maintains the differential mode impedance by creating a highly coupled differential pair that is wound into a coil. Ferrite core might be added to the coil to increase the inductance at lower frequencies. Since a common mode choke is discrete broadband component, it cannot be characterized by its electrical size. There are some other common mode chokes that are manufactured using low-temperature co-fired ceramic (LTCC) substrates with a small size of 1.2 mm ×2.0 mm [3]; these common mode chokes are able to provide common mode suppression up to 5GHz. So far, it is still difficult to find common mode chokes on-board that perform well above 5 GHz. The fourth class of filters are PCB based structures. These resonant structures have been designed to only disturb the common mode field distribution on the differential traces without significantly affecting the differential mode. These structures have been researched well in [4]-[8] by Tzong-Lin Wu's group. Usually the dimension of the resonant structures used for common mode suppression depends on the operating

frequencies. Furthermore, the dimension of the resonators can be reduced by adding PCB structures that act as capacitors or inductors. The PCB structures for common mode suppression usually form narrow-band filters. However, they can be used for wideband applications by combining multiple narrowband filters [9]. Table 2.1 show some examples of PCB structures used for common mode suppression. Electromagnetic band gap (EBG) structures [8] and defected ground structures (DGS) [4] usually occupy large area, which makes them not suitable in practice. Further, it is not clear how defective ground structures perform while there are other planes below them. A structure using quarter wavelength resonator has been proposed in [10], which requires an additional PCB layer, but has a smaller dimension when compared to DGS[4] and EBG[8] structures.

Table 2.1. Comparison of layer number and electrical size.

PCB structure	layer	Normalized
Zigzag geometry and 6 crossings in EBG[9]	2	1.58 λ ×0.50λ
Periodically dumbbell shaped in DGS[4]	2	0.47 λ×0.76λ
U-shaped and H shaped in DGS [8]	2	0.44 λ×0.44 λ
Quarter wave-length resonator[10]	3	0.01 λ×0.25 λ

In this paper, a novel PCB structure for common mode suppression on differential traces is proposed, which is based on the structure reported in [9]. The electrical size of the new PCB structure is only 0.04 λ×0.067λ. Through this design, higher order harmonics of the common mode signal are suppressed. Further, this paper discusses optimization methods and variants of the PCB based common mode filter structure.

2. DESIGN CONCEPT

The basic idea of designing a PCB structure based common mode filter for differential traces is to utilize the different field distributions between the common mode and the differential mode signal. The basic principle is shown in Figure 2.1. Figure 2.1 (a) and (b) illustrate the E and H field distribution of the differential and common mode signals, respectively. Figure 2.1 (c) and (d) show the E and H field distributions after adding a shorting metal plate, between the two traces. The metal plate does not disturb the field distribution of the differential mode, but the field distribution of the common mode is strongly affected because the metal coverts the original perfect magnetic conductor (PMC) boundary condition into a perfect electric conductor (PEC) boundary condition. Therefore, if a quarter-wavelength resonator is placed between the two traces, the resonator will be excited by the common mode signal, but not the differential signal. Thus, the filter structure will only suppress the common mode signal while having little effect on the differential signal.

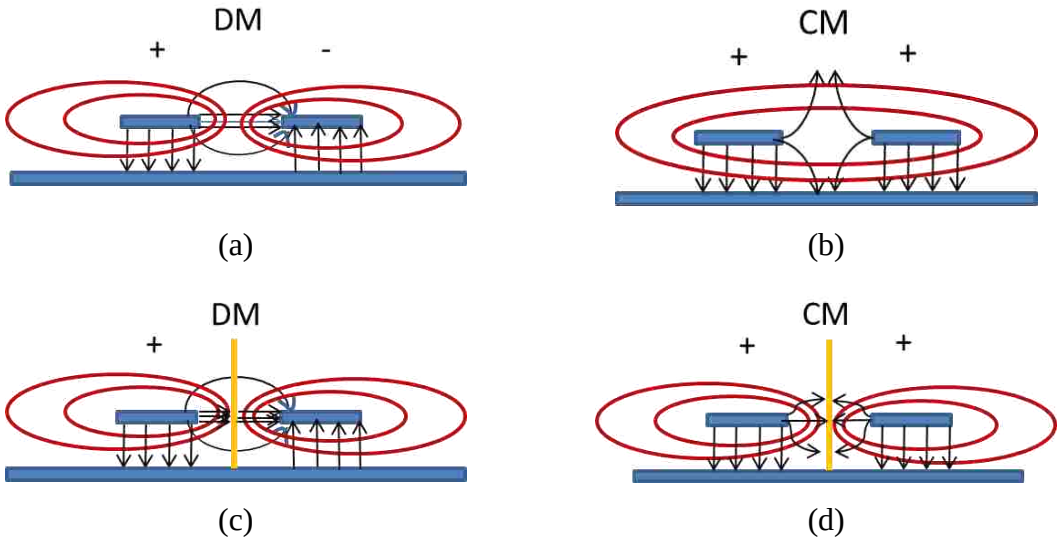

Figure 2.1. (a) E-field and H-field for DM in differential pairs (b) E-field and H-field for CM in differential pairs (c) E-field and H-field for DM in differential pairs after adding a thin metal plane (d) E-field and H-field for CM in differential pairs after adding a thin metal plane

One drawback of the added structure is that it will affect the differential mode impedance. This impedance change can be compensated, however, by modifying the geometry of the differential structure. The next section introduces a basic PCB structure for common mode filtering.

3. BASIC STRUCTURE: QUART WAVELENGTH FILTER

Figure 3.1 shows the basic structure of the common-mode filter in a 3-D view [10]. An extra trace is added in the middle of the two lines of the differential traces. This trace is connected to the ground through a via that located in the middle of the traces. As shown in Figure 3.1 (b), both ends of the extra trace are open, making the structure act as two quarter-wave resonators. The differential mode characteristic impedance is 100 ohms along the traces. The geometry of the differential traces was modified to compensate the resonator's effect on the differential impedance.

The resonant frequency can be calculated as following [10]:

$$f = \frac{c}{4(l + h_{via})\sqrt{\varepsilon_{reff}}} \quad (1)$$

Where ε_{reff} is the effective dielectric constant, represents the length of one resonator, and h_{via} is the height of the via.

The structure shown in Figure 3.1 was fabricated using a 4 layer PCB. The dimension parameters are W=16 mil, S=46.4 mil, L=397.7 mil, Ws=37.6 mil, Z=15.5 mil, and H=9 mil. The dielectric constant, εr, is 4 and the loss tangent is 0.02. According to (1), the resonant frequency of the common mode filter is 4.1 GHz.

Figure 3.2 shows the comparison between the full-wave (HFSS) simulation results and the measurement results. The measurement results agree well with the simulation results. As shown in Figure 3.2, the filter can suppress the common mode signal at 4 GHz while having little effect on the differential mode signal. The total size of the common mode filter is about 0.023λ×0.47λ.

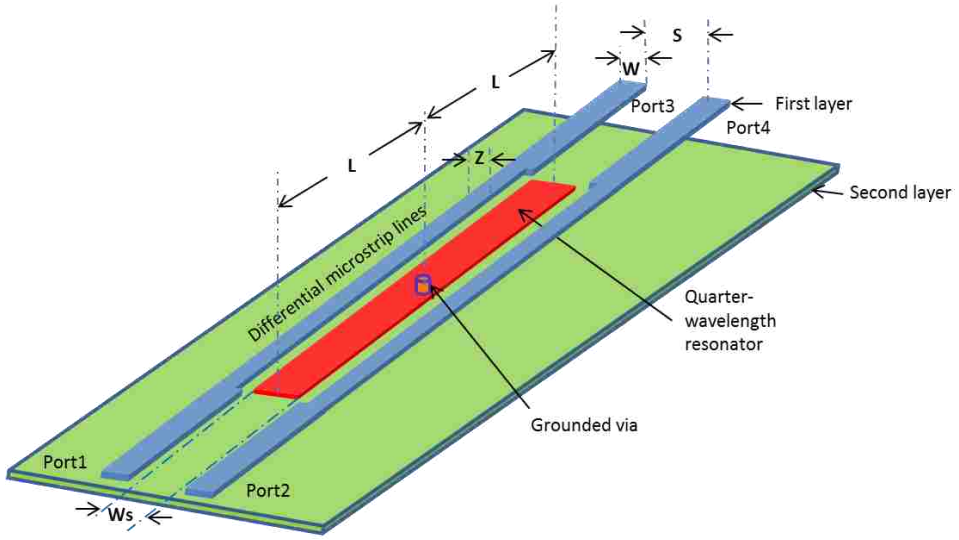

(a)

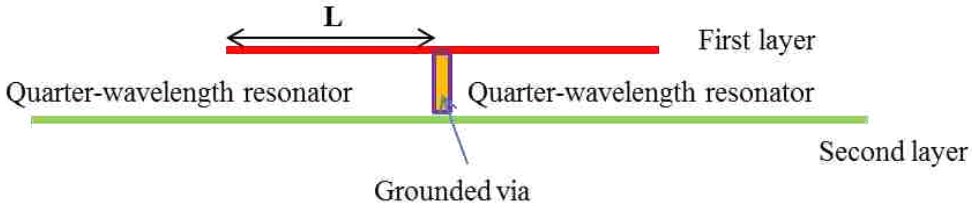

(b)

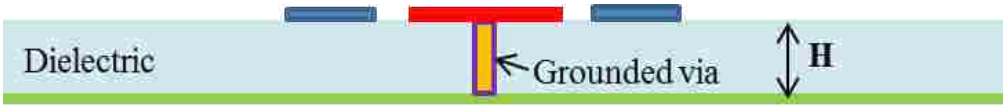

(c)

Figure 3.1. (a) Configuration of common-mode filter in 3-D view (b) Configuration of common-mode filter in cross-section view 1 (c) Configuration of common-mode filter in cross-section view 2.

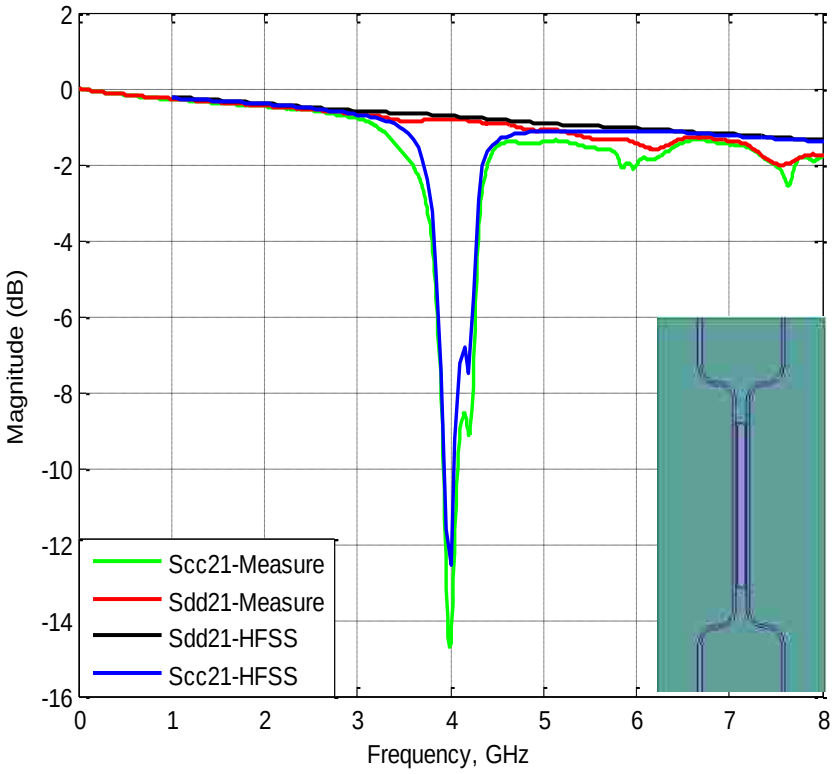

Figure 3.2. Comparisons of the simulation results of S-parameters between full-wave simulation and test PCB board measurement for Figure 3.1.

4. TECHNIQUES FOR REDUCING SIZE

According to (1), it is easy to design a narrow-band common-mode filter at a specified frequency. The longer the quarter-wave resonator is, the lower the resonant frequency. Since smaller structure dimension is desirable in PCB designs, several techniques are introduced in this section to reduce the size of the common mode filter.

4.1. ADDING INTEGRATED CAPACITANCE AT THE END OF THE EXTRA TRACE

Adding capacitors is an effective method to reduce electrical dimension of the filter structure. As shown in Figure 4.1, two 1pF shunt capacitors were added at both ends of the open stub. Due to the loading capacitance at the end of the quarter-wave length resonator, the resonant frequency of the common mode filter is reduced.

Figure 4.2 shows a comparison of the S-parameter measurement results, with and without the loading capacitors. It is evident that after adding the capacitors, the resonant frequency reduces from 3.99 GHz to 2.54 GHz. The occupied area is $0.014\lambda \times 0.29\lambda$, including the loaded capacitors. This comparison demonstrates that adding capacitance is an effective method to reduce the size of the common mode filter. Nevertheless, adding capacitors in this structure will narrow down the relative bandwidth (shown in Table 6.1).

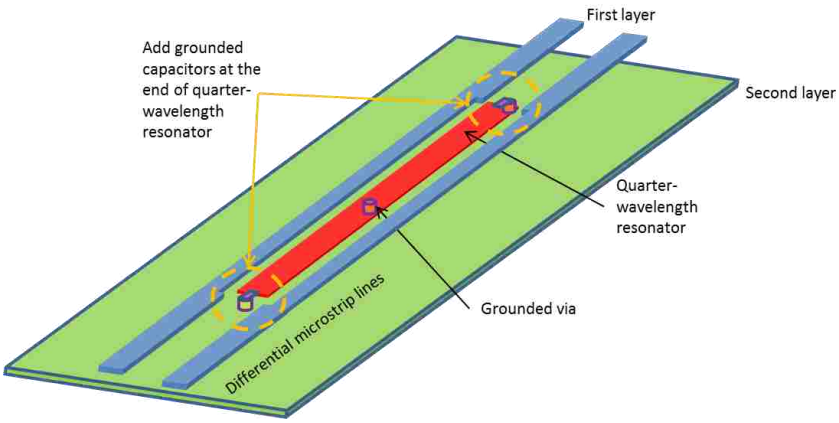

Figure 4.1. Configuration of common-mode filter after adding capacitors at the end of quarter-wavelength resonators in 3-D view.

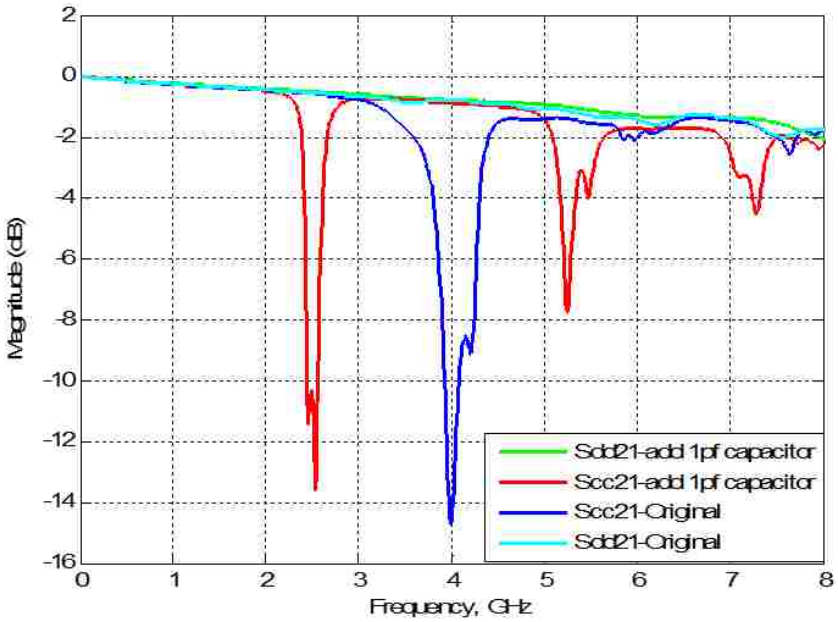

Figure 4.2. Comparison of measured response for normal quarter wavelength resonator structure to the same structure with added 1 pF capacitors.

4.2. RESONATOR UNDERNEATH THE DIFFERENTIAL TRACE

In this variant case, as shown in Figure 4.3, the quarter-wave resonator is placed on the second layer. The third layer is ground plane. The undisturbed second layer ground, which surrounds the resonator, connects the third layer ground by via walls as shown in Figure 4.3 (b). This structure uses one more layer, locally. By doing this, it achieves stronger coupling to the differential trace. The dimensions are W=200 mil, L1=393.7 mil, H1= 40 mil, and H2 = 49 mil. The effective dielectric constant is 4.2. The width of the gap around the resonator is 6 mil. The capacitances at the gaps and to the third layer help to reduce the resonant frequency.

Figure 4.4 shows the simulation results for the common mode filter presented in Figure 4.3. The resonant frequency is 3.1 GHz. In this case, the corresponding electrical size is $0.1\lambda \times 0.2\lambda$. Although the occupied area is larger than the structure shown in Figure 3.1 and Figure 4.1, the bandwidth for this structure is much wider.

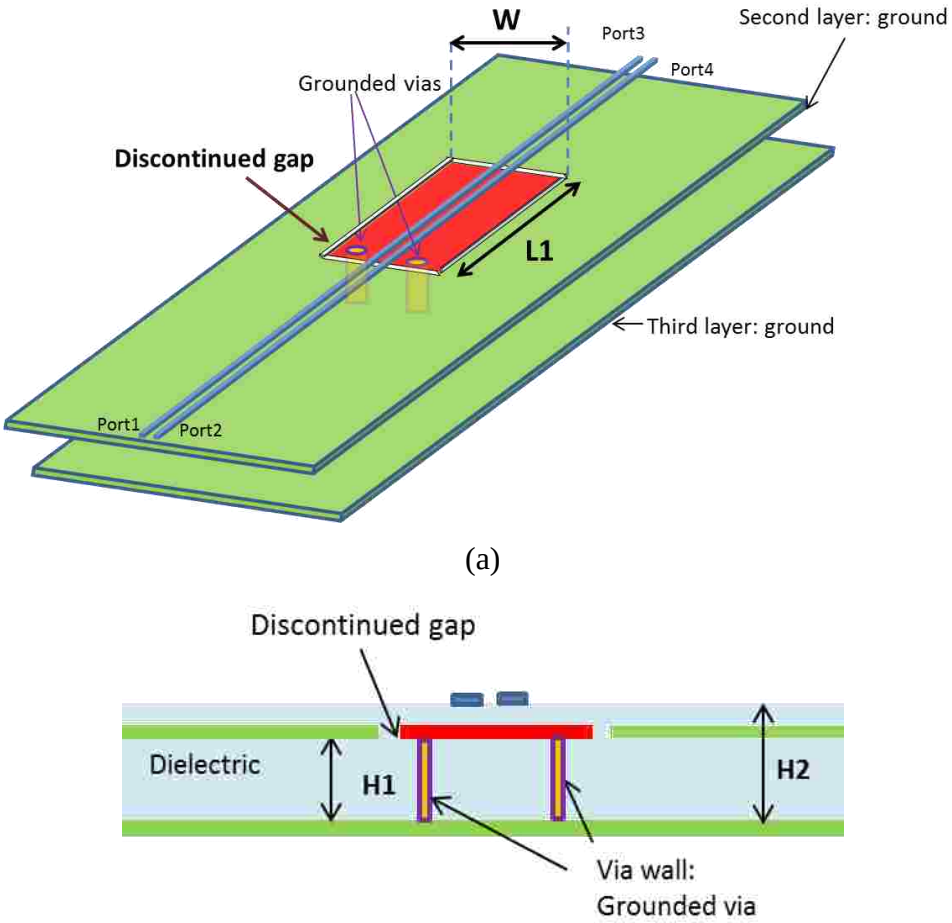

Figure 4.3. (a) Configuration of the common-mode filter in 3-D view (b) Configuration of the common-mode filter in cross-sectional view.

Figure 4.5 (a) shows a modified geometry of the resonator, which increases the inductance to reduce the electrical size of the resonators. Figure 4.5 (b) shows another structure (modified from Figure 3.1 (b)), in which additional traces are added underneath the ground plane using vias. The resonant frequency is reduced by this extra structure. One can view these extensions in the third layer as short transmission lines or as loading capacitors. Both models lead to decreased resonant frequency. This reduces the area of the resonant filter, by occupying another layer.

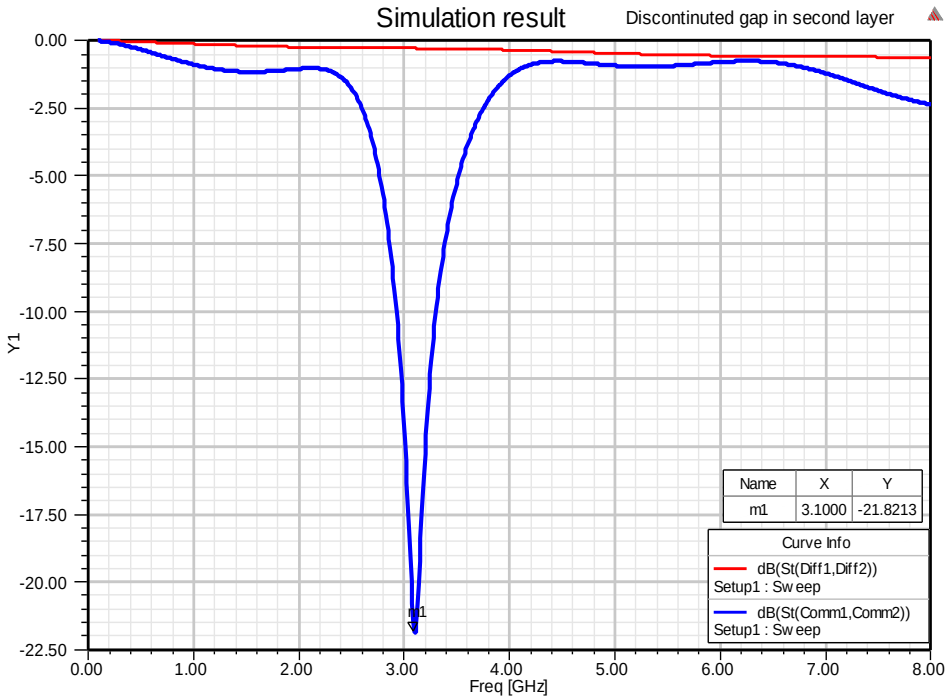

Figure 4.4. Full wave simulated S-parameters for the structure shown in Figure 4.3.

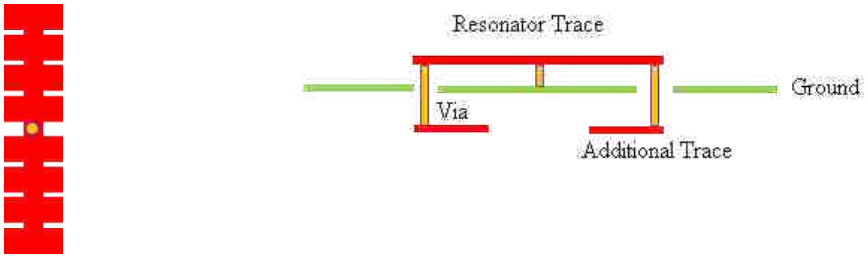

(a) (b)

Figure 4.5. (a) Inductive loaded for resonator and (b) Cross-section for added traces underneath ground plane for reduced resonance frequency.

5. PROPOSED NOVEL STRUCTURE

Based on the techniques discussed above, a new common mode filter structure is proposed, as shown in Figure 5.1. Two resonators are implemented in this structure. The first resonator is placed on the top layer and the second resonator is placed on the second layer. An inter-digital structure is used in the second layer. The ground on the second layer and third layer are connected through a wall of vias. The dimensions are W1=15.5 mil, W2=26 mil, H1=49 mil, H2=40 mil, L1=401.2 mil， L2=370 mil, W3=240 mil, and W4=96 mil.

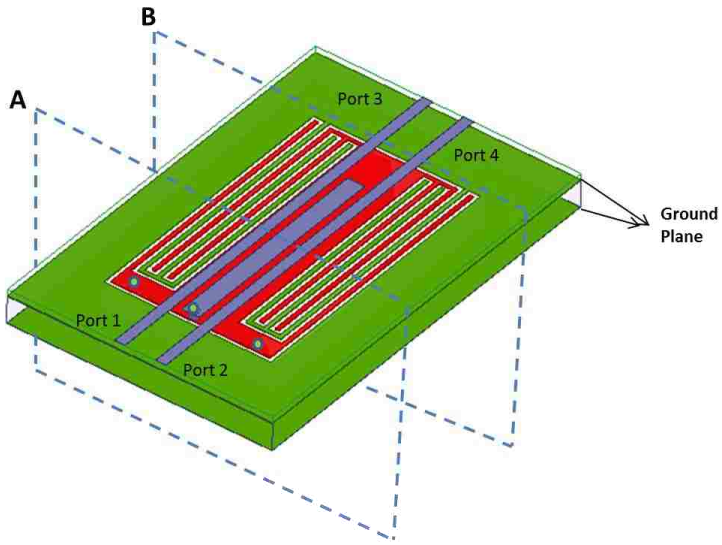

(a)

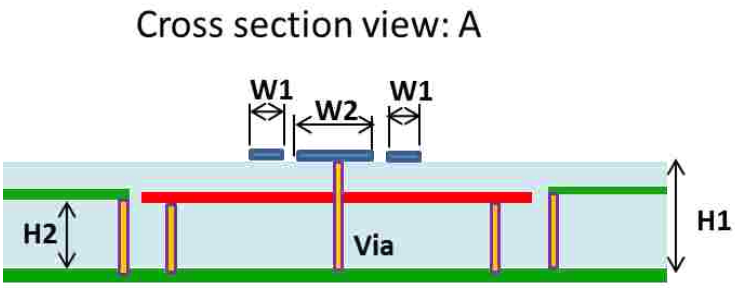

Figure 5.1. (a) Configuration of the new CMF in 3-D view (b) Cross-sectional view (c) Top view for the second layer and (d) Top view of second layer.

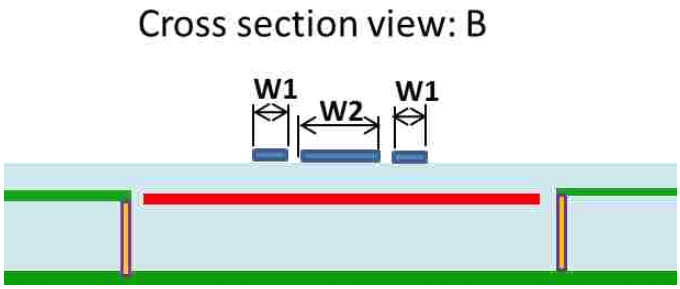

(c)

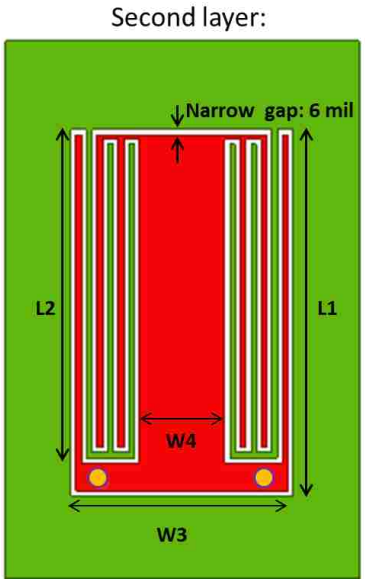

(d)

Figure 5.1. (a) Configuration of the new CMF in 3-D view (b) Cross-sectional view (c) Top view for the second layer and (d) Top view of second layer. (cont).

Figure 5.2 shows the full-wave simulation S-parameter results for the new structure. The first resonant frequency is at 1 GHz, which means the electrical size of the structure is only about $0.04\lambda \times 0.067\lambda$ at this frequency. Moreover, it can suppress common mode noise at additional harmonic frequencies of 2.0GHz, 3.2 GHz, 4.0GHz, 5.1GHz, 5.9GHz, and 6.7GHz, respectively. The effect on the differential signal is trivial which is demonstrated by Sdd in Figure 5.2.

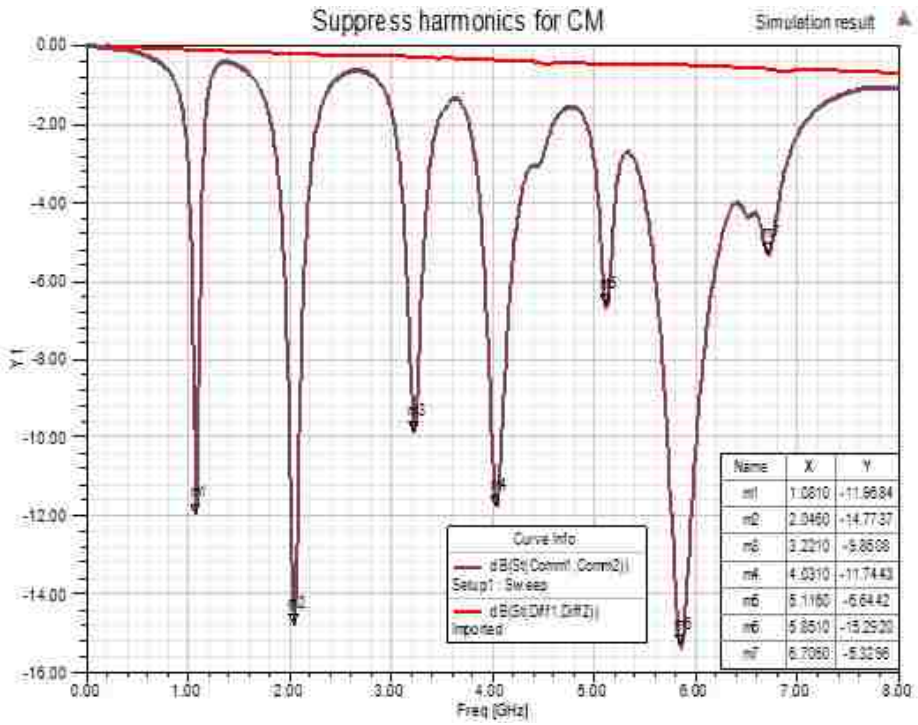

Figure 5.2. Simulation results of the S-parameters from full-wave simulation for the structure shown in Figure 5.1

6. CONCLUSION

PCB based resonant structures can suppress common mode noise on differential traces. Optimization criteria are the electrical dimension (expressed in fractions of a wavelength), the number of layers to implement the structures, the PCB manufacturing constraints, and the resulting frequency responses. The common-mode filter can be narrow-band (for suppressing a specific frequency) or wideband if several narrow-band filters are combined together. Several techniques for reducing the electrical size of common mode filters are discussed and applied in the new design. The new structure has a very small electrical size at its first resonant frequency. The electrical sizes and the bandwidths are shown for different structures in Table 6.1. Another further advantage of the proposed structure is its capability to suppress higher order harmonics, while a quarter wavelength resonator will only suppress harmonics at the fundamental and 3rd, 5th, and 7th order of harmonics, with the absence of the second harmonic, which often shows up strongly when analyzing the harmonics of unwanted common mode signals in a differential channel.

Table 6.1. Comparison of layer number and electrical size.

PCB structure	layer	Bandwidth	Normalized
Figure 3.1	2	17.5%	0.023 λ ×0.47λ
Figure.4.1	2	12%	0.014 λ ×0.29λ
Figure 4.3	3	38.7%	0.1 λ ×0.2λ
Figure 5.1	3	20%	0.04 λ ×0.067 λ

REFERENCES

[1] C. Chang, R. Fang, C. Wang, “Bended Differential transmission line using compensation inductance for common-mode noise suppression”, IEEE Trans. Comp., Packag. Manf. Technol. vol. 2, pp. 1518-1525, Sep. 2012.

[2] C. Chang, R. Fang, C. Wang, “Bended Differential transmission line using compensation inductance for common-mode noise suppression”, IEEE Trans. Comp., Packag. Manf. Technol. vol. 2, pp. 1518-1525, Sep. 2012.

[3] Chung-Hao Tsai; Jing-Zuei Hsu; Iat-In Ao Ieong; Tzong-Lin Wu, "A novel common mode choke and its application for 5 Gbps USB 3.0," Electromagnetic Compatibility (EMC), 2011 IEEE International Symposium on , vol., no., pp.888,891, 14-19 Aug. 2011.

[4] Wei-Tzong Liu; Chung-Hao Tsai; Tzu-Wei Han; Tzong-Lin Wu, "An Embedded Common-Mode Suppression Filter for GHz Differential Signals Using Periodic Defected Ground Plane," Microwave and Wireless Components Letters, IEEE , vol.18, no.4, pp.248,250, April 2008.

[5] Chih-Ying Hsiao; Chung-Hao Tsai; Cheng-Nan Chiu; Tzong-Lin Wu, "Radiation Suppression for Cable-Attached Packages Utilizing a Compact Embedded Common-Mode Filter," Components, Packaging and Manufacturing Technology, IEEE Transactions on , vol.2, no.10, pp.1696,1703, Oct. 2012.

[6] Hao-Hsiang Chuang; Tzong-Lin Wu, "A Novel Ground Resonator Technique to Reduce Common-Mode Radiation on Slot-Crossing Differential Signals," Microwave and Wireless Components Letters, IEEE , vol.20, no.12, pp.660,662, Dec. 2010.

[7] Jui-Chih Yen; Sen-Kuei Hsu; Tong-Hong Lin; Tzong-Lin Wu, "A Broadband Forward-Wave Directional Coupler Using Periodic Y-Shaped Ground Via Structures With Arbitrary Coupling Levels," Microwave Theory and Techniques, IEEE Transactions on, vol.61, no.1, pp.38,47, Jan. 2013.

[8] Wu, T.-L.; Chung-Hao Tsai; Tzong-Lin Wu; Itoh, T., "A Novel Wideband Common-Mode Suppression Filter for Gigahertz Differential Signals Using Coupled Patterned Ground Structure," Microwave Theory and Techniques, IEEE Transactions on , vol.57, no.4, pp.848,855, April 2009.

[9] de Paulis, F.; Raimondo, L.; Connor, S.; Archambeault, B.; Orlandi, A., "Compact Configuration for Common Mode Filter Design based on Planar Electromagnetic Bandgap Structures," Electromagnetic Compatibility, IEEE Transactions on , vol.54, no.3, pp.646,654, June 2012.

[10] Shiue, G.-H.; Hsu, C.-M.; Yeh, C.-L.; Hsu, C.-F., "A Comprehensive Investigation of a Common-Mode Filter for Gigahertz Differential Signals Using Quarter-Wavelength Resonators," Components, Packaging and Manufacturing Technology, IEEE Transactions on , vol.4, no.1, pp.134,144, Jan. 2013.

IV. MODELING ABSORBING MATERIALS FOR EMI MITIGATION

Qian Liu, Xiangyang Jiao, Jing Li, Victor Khilkevich, James Drewniak, Paul Dixon, Yoeri Arien

ABSTRACT

In this study, the parameters of magnetic absorbing materials were measured and used to predict their effectiveness at reducing total radiation power from a Heatsinks. The parameters of absorbing materials were measured using a transmission line method and fitted using the Debye model. By comparing S-parameters and power loss between a simulated and measured microstrip line, the fitted material parameters were validated. The heatsink model has also been investigated to determine the radiation mitigation with lossy materials.

Index Terms— Absorbing material; parameter validation; microstrip line; heatsink.

1. INTRODUCTION

Absorbing materials, commonly referred to as lossy materials, are widely used in practical engineering areas. Lossy materials can be applied for electromagnetic noise-suppressing or emission-suppressing in electronic devices or systems in order to satisfy the standards of electromagnetic compatibility [1-2].

It is necessary to know the permeability (μ) and permittivity (ε) of the lossy material to be able to choose the appropriate material from a number of available candidates and predict the performance of the EMI mitigation solution. There are many methods to get material properties [3-4], such as transmission/reflection method, resonant method and planar-circuit methods. Due to different material types, frequency range, and instrument availability, different methods might be applied. The transmission line methods are based on measuring S-parameters of networks under test and have a broad frequency range, which makes these transmission line methods preferable for many applications. Any available material parameter measurement technique allows for extracting material parameters within some accuracy limits, which makes validation of measured parameters an important task.

For a high speed system, once the EMI source is identified, a suitable volume of absorber material can be placed on the source location to reduce the radiated power at the frequency of interest. For example, a heatsink is usually placed over a chip pakage for heat dissipation. The heatsink is typically metallic and is in close proximity to a major energy source—the chip–which leads to increased radiation [5-6]. If the absorber parameters are known and the heatsink model is available, it becomes possible to determine the needed volume and configuration of the absorber to achieve the most efficient usage of the material.

In the study, relative permeability (μ_r) and permittivity (ε_r) of the absorber are obtained using a transmission line method. A microstrip transmission line with lossy material placed above the trace is used to validate the material properties. Furthermore, the application of absorber material to mitigate the radiation of heatsink has also been investigated.

2. MEASUREMENT OF MATERIAL PARAMETERS

Material properties in the frequency range of interest can be measured using a transmission line technique [7]. The type of the transmission line was choosen depending on the freqeuncy range as shown in Table 2.1.

Table 2.1. Coaxial/waveguide fixtures.

Set up	Frequency range	Simple size
Coax∅=3 1/8”	0 - 2.4GHz	outer∅: 76.8+0/-0.1, inner∅: 33.35-0/+0.1
Coax∅=7/8”	0 - 6.5GHz	outer∅: 19.87+0/-0.1, inner∅: 8.7-0/+0.1
S-band Waveguide	2.6 - 4GHz	34.10 -0/+0.1, 72.20 -0/+0.1mm
X-band Waveguide	8 - 12.5GHz	7.89 -0/+0.1, 22.83 -0/+0.1mm
Ku-band Waveguide	12.5 - 18GHz	7.89 -0/+0.1, 15.81 -0/+0.1mm
J/K-band Waveguide	18 - 26.5GHz	10.65 -0/+0.1, 4.31 -0/+0.1mm

In this study, two different flexible magnetic lossy materials (material A and B) were measured by combining the waveguide and coaxial line methods. Figure 2.1 and Figure 2.2 show the parameters of materials A and B, respectively. The real and imaginary parts of μ_r and ε_r in physical materials have to satisfy the Kramers-Kroning relations, which is achieved by fitting the obtained curves to the Debye model. The measured data was imported to the FEMAS software [8] to perform the fitting, shown in Figure 2.1 and Figure 2.2. The measurement results were then compared to the fitted results. With high-order Debye model fitting, it becomes possible to approximate measured curves relatively accurately.

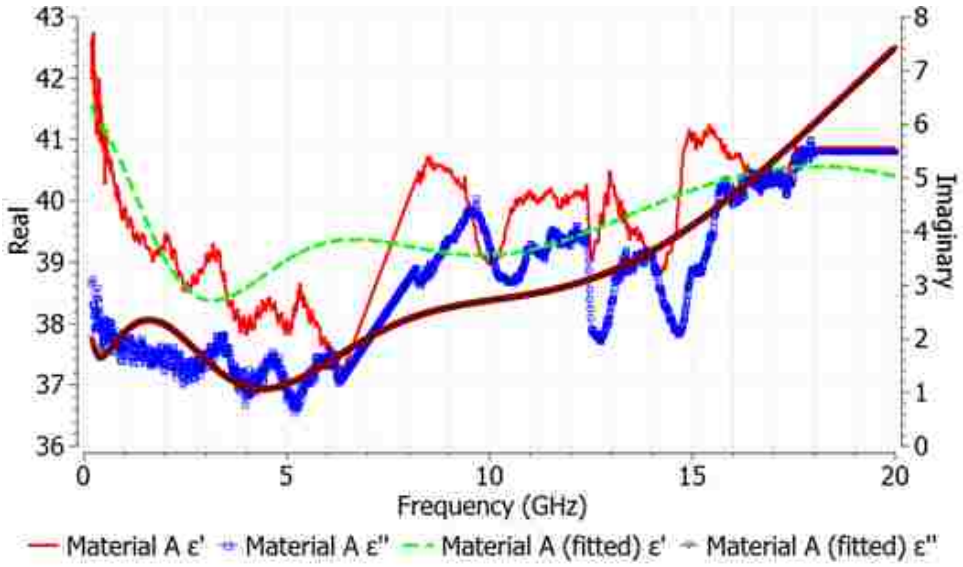

(a)

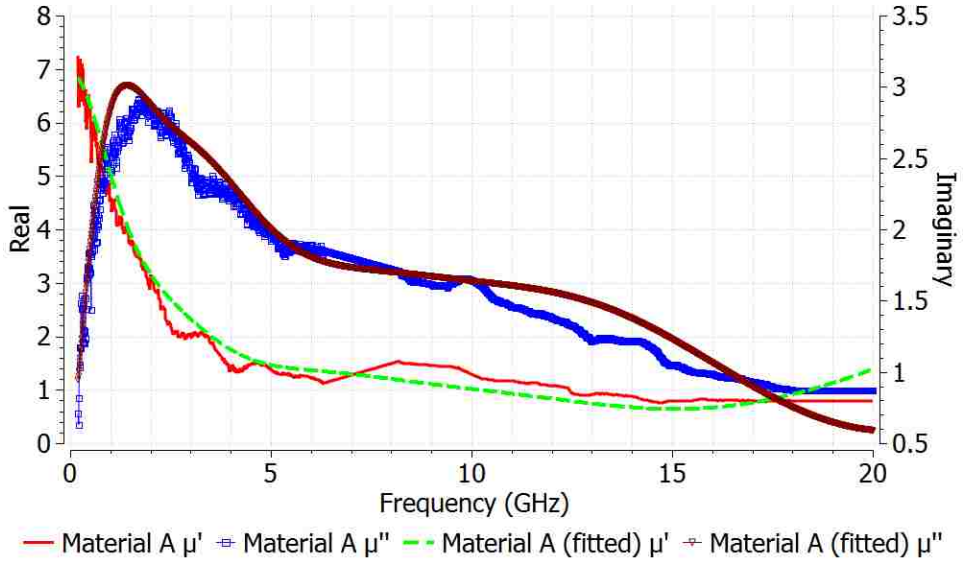

(b)

Figure 2.1. The permittivity (a) and permibility (b) of Material A: measurement results and the multi-term Debye model curve fitting.

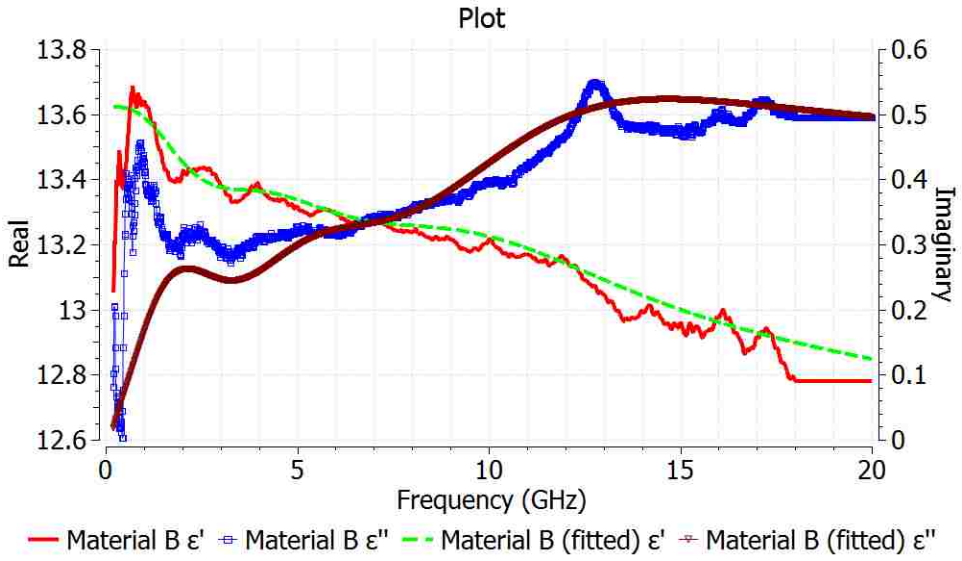

(a)

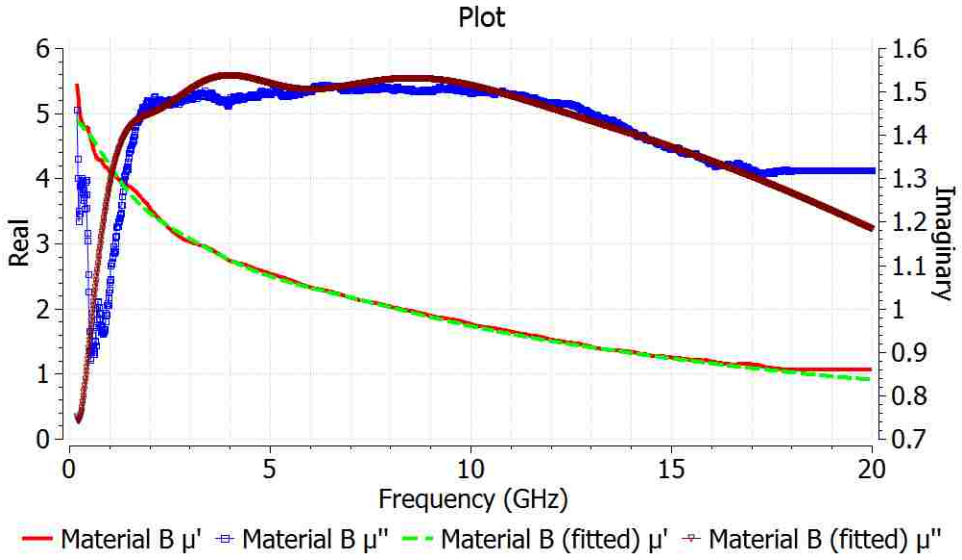

(b)

Figure 2.2. The permittivity (a) and permeability (b) of material B: measurement results and the multi-term Debye model curve fitting

3. MODELING MICROSTRIP LINE FOR VALIDATION MATERIAL PROPERTIES

A simple way to validate the measured parameters of lossy material is to apply the material to a microstrip line and observe its influence on the S-parameters of the line. Figure 3.1 shows the test PCB used for the validation. The microstrip line is manufactured on a low loss substrate and contains a pattern for a TRL calibration. The measured and simulated S-parameters and power loss of the line without additional absorber are compared in Figure 3.2. The power loss is defined as the sum of the radiation loss and total material loss and can be calculated as follows [9]:

$$P_{loss} = (1/2)[\vec{a}]^t([\tilde{I}] - [\tilde{s}]^t[\tilde{s}])[\vec{a}] \quad (1)$$

where is an incident power wave vector with units of , t denotes the complex conjugate transpose, is the identity matrix, and is the S-parameter matrix. As can be seen from Figure 3.2, the model provides good agreement with the measurement, which validates the microstrip line model.

After the validation of the microstrip line model, the lossy material with previously measured parameters was added to the model to validate the material property measurement. Figure 3.3 shows the measurement setup with lossy material B (Figure 2.2) placed on the trace. A clamp was used to put pressure on the material for the purpose of minimizing the air gap between the microstrip and material. This is needed to ensure good measurement repeatability.

Figure 3.1. Variation of emissions from cables under CM and DM excitations.

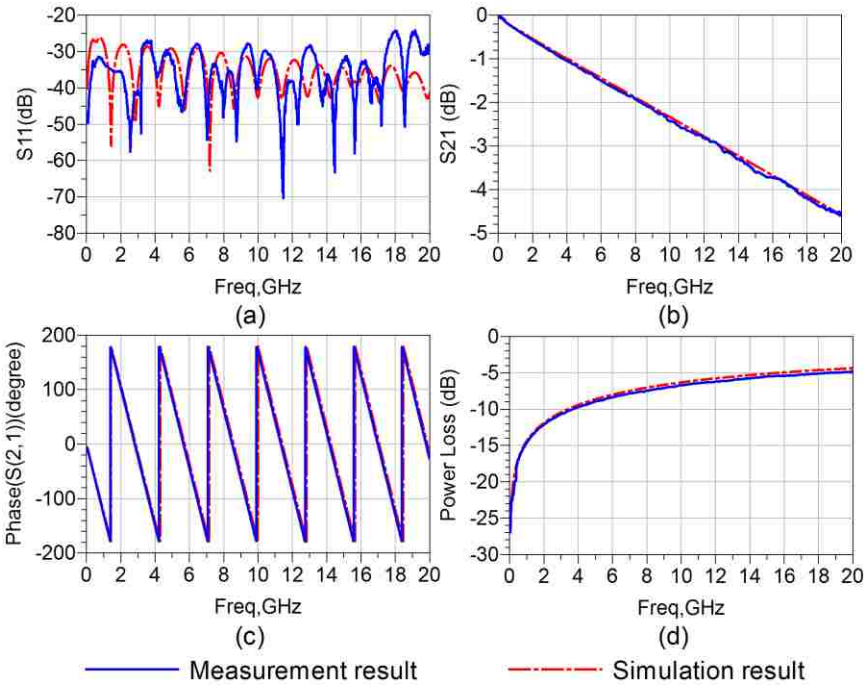

Figure 3.2. The comparison between simulation and measurement for the microstrip line.

The setup was simulated using the time-domain solver of CST Microwave Studio shown in Figure 3.4[10]. The Debye model of the measured absorbing material parameters was imported. Figure 3.5 shows the simulation and measurement results after applying lossy material B to the microstrip. Figure 3.5 demonstrates good agreement between the measured and simulated data, which validates the measured material properties.

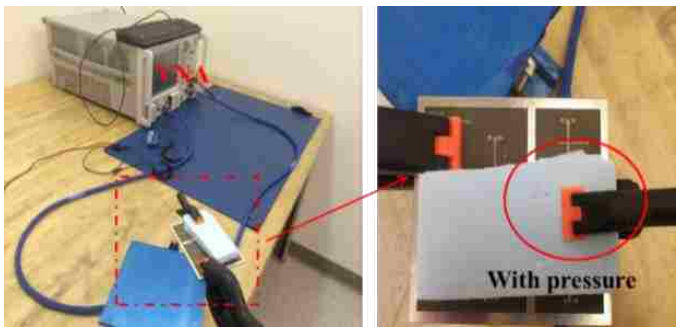

Figure 3.3. S-parameters measurement setup for determining lossy material properties.

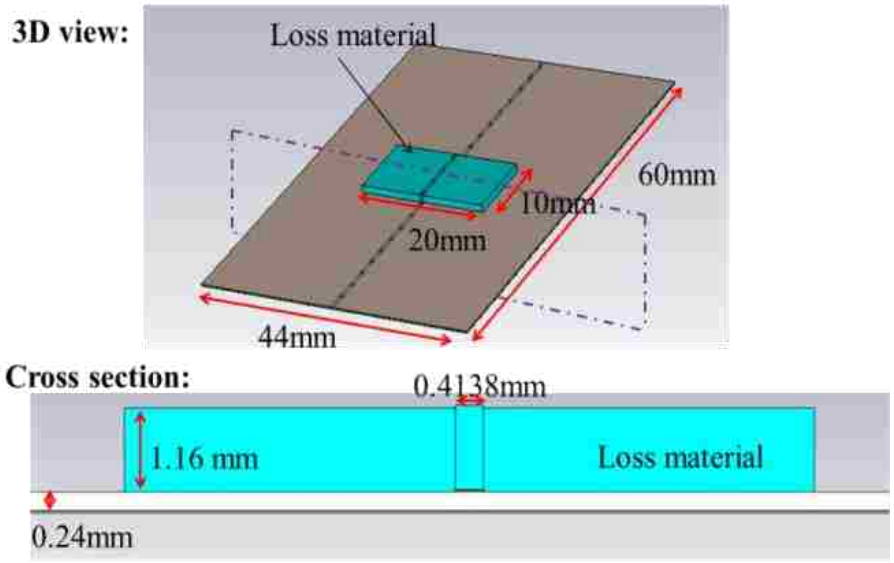

Figure 3.4. CST Microwave Studio model of mocristrip line with lossy material.

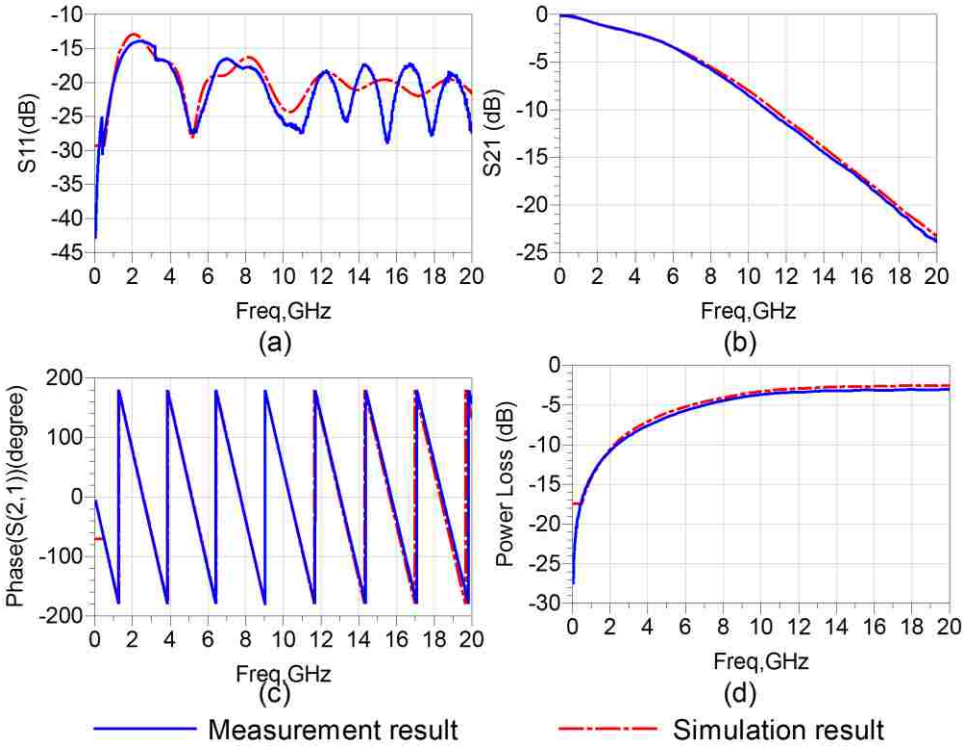

Figure 3.5. The comparison between simulation and measurement for the microstrip line with lossy material.

4. APPLICATION TO THE HEATSINK

Absorbing materials can be used for EMI mitigation purposes. A suitable volume of absorber material might be placed on the source location (e.g., a heatsink) to reduce the radiated power. Figure 4.1 shows the side view of the test fixture used in this study. The heatsink was put 3 mm above the ground plane over a 20x20 mm patch antenna, which was driven by an SMA connector.

The test fixture was used to measure the EMI mitigation effectiveness of the absorbers applied to the heatsink. In this particular test, a "picture-frame" absorber was added around the exciting patch antenna. The CST Microwave Studio model of the test fixture was also assembled for further validation of the measured material properties (Figure 4.2). In the model, a far field monitor was added to calculate the total radiated power with 1 Watt input power.

The effectiveness of the absorber is assessed in terms of the total radiated power, which is measured in the reverberation chamber.

According to [11], the total (transmitted) radiated power of the heat sink P_T^H can be found as:

$$\langle P_T^H \rangle = \frac{\langle P_T^A \rangle}{\langle P_R^H \rangle} \langle P_R^H \rangle \tag{2}$$

The measurement is done in two stages. During the first stage (calibration) the power P_T^A is applied to one of the calibration antennas and the power P_R^A is received by another antenna. During the measurement, the power emitted by the heatsink (P_R^H) is measured by one of the antennas used in the calibration. In the formula (2), the symbol $\langle\rangle$ denotes averaging over the range of steerer positions. If the measurements are performed with VNA excitation, and well matched antennas are used, equation (2) can be changed to [12]:

$$\langle P_T^H \rangle \approx \frac{\langle S_{21}^H \rangle}{\langle S_{21}^A \rangle} \langle P_{in}^H \rangle \tag{3}$$

Where S_{21}^{A} is the transmission coefficient between two calibration antennas (shown in Figure 4.3) and S_{21}^{H} is the transmission coefficient between the heat sink and one of the antennas (shown in Figure 4.4), and P_{in}^{H} is the assumed power applied to the heatsink.

Figure 4.1. Side view of measured heatsink with square metal patch as the excitation.

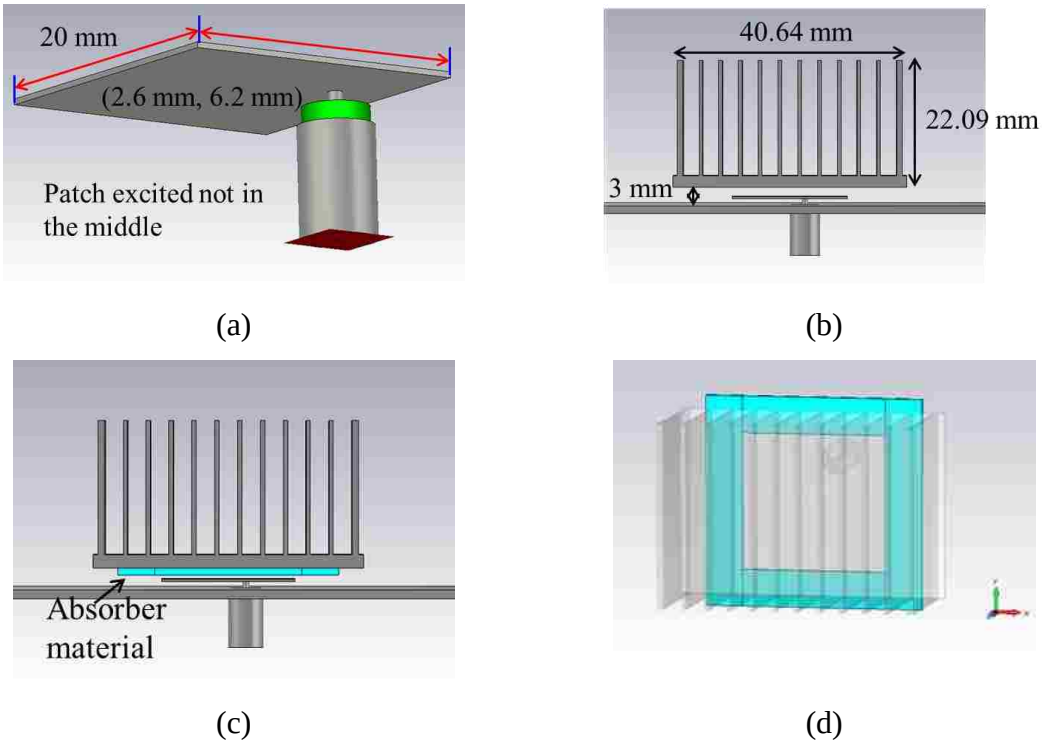

Figure 4.2. CST Microwave Studio model: (a) patch between the ground and heatsink (b) cross section view of the model (c) a picture frame absober is added to the bottem of the heatsink (d) picture frame lossy material

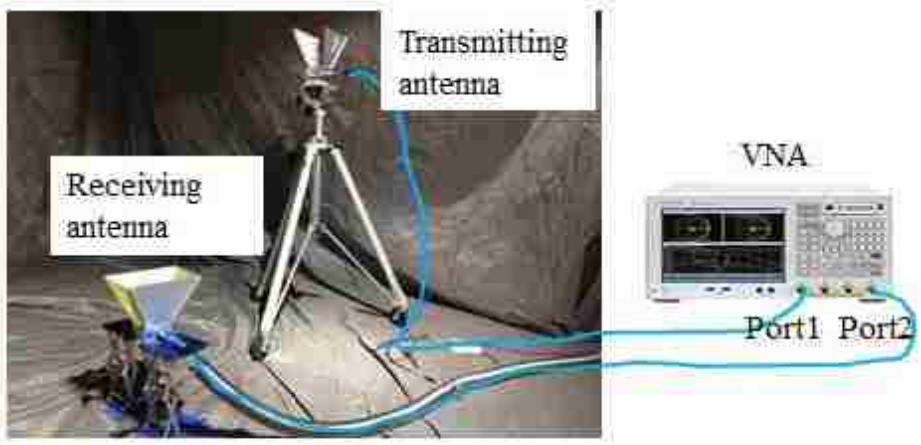

Figure 4.3. Setup for chamber calibration.

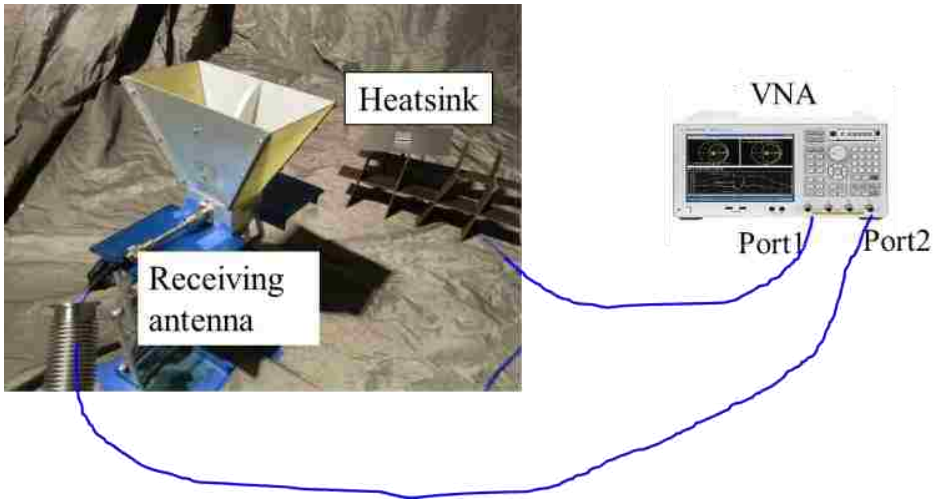

Figure 4.4. Setup for total radiation measurement.

The simulated and measured values of the TRP are shown in Figure 4.5. The measured TRP in Figure 4.5 was renormalized to 1 Watt excitation for the comaprison purposes. The curves of EMI reduction (shielding effectiveness) due to the added lossy material obtained in measurement and simulation are shown in Figure 4.6. The difference between the measured and simulated TRP reduction figures does not exceed 6.5 dB, and is 2.3 dB on average. This result allows one to predict the EMI performance of the absorbing materials with high conficence. At the same time, it should be noted that the

measured and calculated shielding effectiveness curves are specific to the particular excitation type (e.g., a patch antenna) and might be different for different excitaton mechanisms (e.g., a magnetic loop or a monopole).

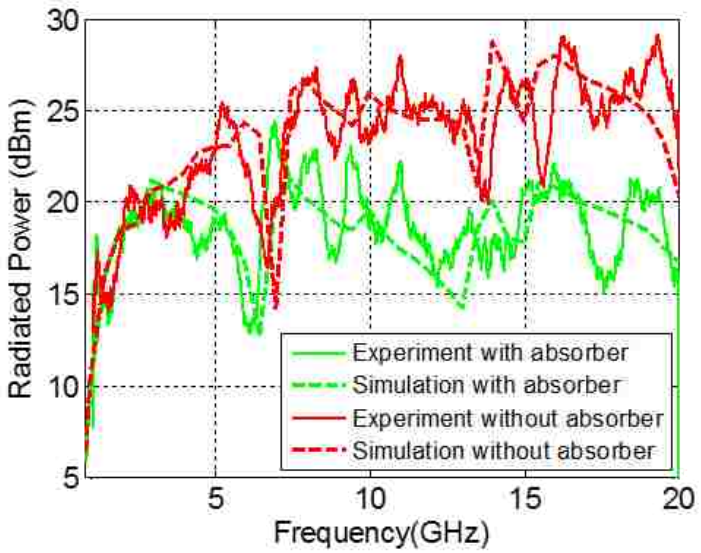

Figure 4.5. Comparison of simulated and measured results of radiation power.

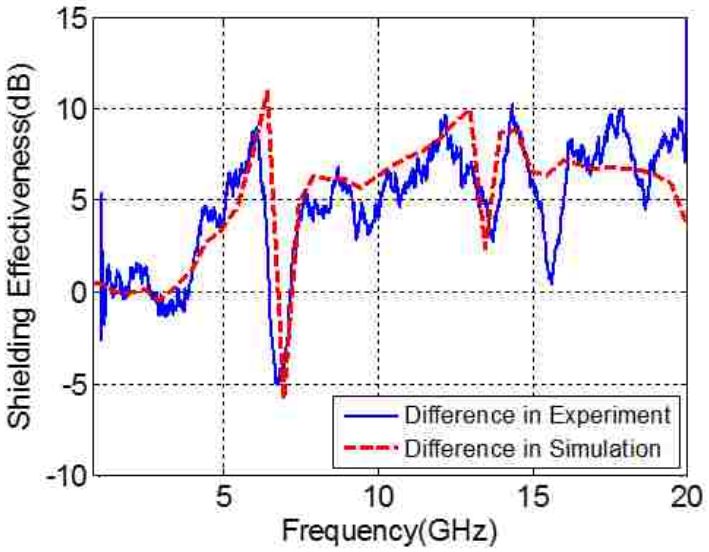

Figure 4.6. Comparison of simulated and measured results of total radiation reduction (shielding effectiveness).

5. CONCLUSION

The transmission line measurement method allows measuring the material parameters of flexible magnetic absorbers with relatively good accuracy. The measurement was validated by the microstrip line measurement and in the heatsink test fixture. The microstrip line test can be recommended as an easy-to-implement validation method for the measured material parameters.

The whole measurement and simulation procedure allows predicting the EMI mitigation performance of magnetic absorbers with an average accuracy of approximately 2 dB, which makes it accurate enough for practical EMC applications.

REFERENCES

[1] Jing Li; Koledintseva, M.Y.; Razmadze, A.; Gafarov, A.; Yao-Jiang Zhang; Drewniak, J.L.; Jun Fan; Shenhui, J., "Permeability and permittivity uncertainty effects in modeling absorbing coatings and ferrites on cables," Electromagnetic Compatibility (EMC), 2012 IEEE International Symposium on , vol., no., pp.74,79, 6-10 Aug. 2012.

[2] J. Li, Y.-J. Zhang, A. Gafarov, S. De, M. Koledintseva, J. Marchand, D. Hess, T. Durant, J. Drewniak, and J. Fan, "EMI reduction evaluation with flexible absorbing materials and ferrite cores applied on cables", Proc. IEEE Symp. Electromag. Compat., Pittsburg, PA, Aug. 5-10, 2012.

[3] L.F. Chen, C.K. Ong, C.P. Neo, V.V. Varadan, and V.K. Varadan, Microwave Electronics – Measurement and Material Characterisation, Wiley, 2004.

[4] Bush Space Company, Gary G., "Measurement techniques for permeability, permittivity and EMI shielding: a review," Electromagnetic Compatibility, 1994. Symposium Record. Compatibility in the Loop., IEEE International Symposium on , vol., no., pp.333,339, 22-26 Aug 1994.

[5] X. Zhou, Jing Li, H. Fan, A. Bhobe, K. Taunk, J. Yu, P. Sochoux, "Validating EMC Simulation by Measurement in Reverberation Chamber," Designcon 2013, San Jose, CA, January 28-31, 2013.

[6] X. Zhou, Jing. Li, H. Fan, A. Bhobe, P. Sochoux, J. Yu, "High-frequency EMC design verification through full-wave simulations and measurements in Reverberation Chamber," in proceedings of IEEE International Symposium on Electromagnetic Compatibility, Denver, CO, Aug. 2013, pp. 299-305.

[7] Baker-Jarvis and etal, "Measuring the permittivity and permeability of lossy materials: solid, liquids, metals, building materials and negative -index materials," NIST technical note 1536, Feb. 2005.

[8] http://www.ems-plus.com/FEMAS_main.html.

[9] X. Tian, M. S. Halligan, X. Li, K. Kim, H.-C. Chen, S. Connor, B. Archambeault, M. Cracraft, A. E. Ruehli, and J. L. Drewniak, "Modeling electromagnetic radiation at high-density PCB/connector interfaces," presented at the IEEE Int. Symp. Electromagn. Compat., Raleigh, NC, USA, Aug. 2014.

[10] CST MICROWAVE STUDIO. ver. 13, CST Computer Simulation Technology, Available: https://www.cst.com/.

[11] G. Koepke and J. Ladbury, “Radiated Power Measurements in Reverberation Chambers,” 56th ARFTG Conference Digest-Fall, vol.38, pp.1-7, 2000.

[12] Holloway, C.L.; Hill, D.A.; Sandroni, M.; Ladbury, J.M.; Coder, J.; Koepke, G.; Marvin, A.C.; Yuhui He, "Use of Reverberation Chambers to Determine the Shielding Effectiveness of Physically Small, Electrically Large Enclosures and Cavities," Electromagnetic Compatibility, IEEE Transactions on , vol.50, no.4, pp.770,782, Nov. 2008.

SECTION

2. CONCLUSIONS

Paper I, Paper II and Paper III show three common mode filters. The advantages of the filter are numerous. PCB embedded filter can be put into PCB and easy to manufacture. Removable EBG filter can be installed, substituted and removed by the typical soldering assembly process, which is easy to meet the filter needs of PCB differential link designers at any stage of the design process.

Paper IV shows transmission line measurement method to validate the material parameters of flexible magnetic absorbers with relatively good accuracy. The measurement was validated by the microstrip line measurement and in the heatsink test fixture. The microstrip line test can be recommended as an easy-to-implement validation method for the measured material parameters.

VITA

Qian Liu was born in Guangxi Province, P. R. China, 1990. She received the B.S. degree in electrical engineering from the University of Electronic Science and Technology of China, Chengdu, China, in 2013. In 2013 fall, she started her Master in the Electrical and Computer Engineering Department at Missouri University of Science and Technology. She has also worked as a fall Co-op at IBM Systems Group during Jun.-Dec. 2015. She received her Master degree in July 2016 from Missouri University of Science and Technology.